Title page

HACD1, a regulator of membrane composition and fluidity, promotes myoblast fusion and skeletal muscle growth

Jordan Blondelle[1,2,3,4], Yusuke Ohno[5,*], Vincent Gache[1,2,3,4,*], Stéphane Guyot[6], Sébastien Storck[7], Nicolas Blanchard-Gutton[1,2,3,4], Inès Barthélémy[1,2,3,4], Gemma Walmsley[8], Anaëlle Rahier[1,2,3,4], Stéphanie Gadin[1,2,3,4], Marie Maurer[1,2,3,4], Laurent Guillaud[1,2,3,4], Alexandre Prola[1,2,3,4], Arnaud Ferry[9], Geneviève Aubin-Houzelstein[1,2,3,4], Jean Demarquoy[10], Frédéric Relaix[1,2,3,4], Richard J. Piercy[8], Stéphane Blot[1,2,3,4], Akio Kihara[5], Laurent Tiret[1,2,3,4,¶], and Fanny Pilot-Storck[1,2,3,4,¶]

1 Inserm, IMRB U955-E10, 94000 Créteil, France
2 Université Paris-Est, Ecole nationale vétérinaire d'Alfort, 94700, Maisons-Alfort, & Faculté de médecine, 94000 Créteil, France
3 APHP, Hopitaux Universitaires Henri Mondor, DHU Pepsy & Centre de référence des maladies neuromusculaires GNMH, 94000 Créteil, France
4 Etablissement Français du Sang, 94017 Créteil, France
5 Laboratory of Biochemistry, Faculty of Pharmaceutical Sciences, Hokkaido University, Sapporo 060-0812, Japan.
6 UMR A 02.102 Procédés Alimentaires et Microbiologiques, équipe Procédés Microbiologiques et Biotechnologiques, AgroSup Dijon / Université de Bourgogne, 21000 Dijon, France.
7 Institut Necker-Enfants Malades, INSERM U1151-CNRS UMR 8253, Université Paris Descartes, Sorbonne Paris Cité, Faculté de médecine, site Broussais, 75000 Paris, France.
8 Comparative Neuromuscular Disease Laboratory, Department of Clinical Sciences and Services, Royal Veterinary College, London, NW1 0TU, United Kingdom.
9 Thérapie des maladies du muscle strié INSERM U974 - CNRS UMR7215 - UPMC UM76 - Institut de Myologie, Université Pierre et Marie Curie, and Université Paris Descartes, 75000 Paris, France.
10 Laboratoire Bio-PeroxIL, Biochimie du Peroxysome, Inflammation et Métabolisme Lipidique, Université de Bourgogne - Faculté des Sciences Gabriel, 21000 Dijon, France.

[*] These authors contributed equally to this work
[¶] Co-corresponding authors

Correspondence to: Fanny Pilot-Storck or Laurent Tiret
Ecole nationale vétérinaire d'Alfort, 7 avenue du général de Gaulle
94700 Maisons-Alfort, France.
E-mail: fstorck@vet-alfort.fr or ltiret@vet-alfort.fr
Tel: +33 1 43 96 72 75 – Fax: +33 1 43 96 71 69

Running title: HACD1 promotes myoblast fusion

Author Contributions: FPS, LT, AK, SB, JD, GAH and RJP designed research. JB, YO, VG, SG, SS, NBG, IB, GW, AR, SG, MM, LG, AP, AF, SB and FPS performed research. FPS, JB, VG, AP, LT, FR, AK, YO, JD, SS and SB analyzed the data. FPS, JB, VG and LT wrote the manuscript and RJP edited the manuscript. The authors declare that they have no conflict of interest.

Abstract

The reduced diameter of skeletal myofibres is a hallmark of several congenital myopathies, yet the underlying cellular and molecular mechanisms remain elusive. In this study we investigated the role of *HACD1/PTPLA*, involved in the elongation of the very long chain fatty acids, in muscle fibre formation. In humans and dogs, HACD1 deficiency leads to a congenital myopathy with fibre size disproportion associated with a generalized muscle weakness. Through analysis of HACD1-deficient Labradors, *Hacd1*-knockout mice and *Hacd1*-deficient myoblasts, we provide here evidence that HACD1 promotes myoblast fusion during muscle development and regeneration. We further demonstrated that in normal differentiating myoblasts, expression of the catalytically active HACD1 isoform, encoded by a muscle-enriched splice variant, yields a decrease in lysophosphatidylcholine content, a potent inhibitor of myoblast fusion, and an increase in concentrations of ≥C18 and monounsaturated fatty acids of phospholipids. These lipid modifications correlated with a reduction in plasma membrane rigidity. In conclusion, we propose that fusion impairement constitutes a novel, non-exclusive pathological mechanism operating in congenital myopathies and reveal that *HACD1* is a key regulator of a lipid-dependent muscle fibre growth mechanism.

Keywords:

Centronuclear myopathy; LPC; MUFA; Protein Tyrosine Phosphatase-like, member A; VLCFA

Abbreviations:

CNM = centronuclear myopathy

Main Text

Introduction

Congenital myopathies are rare hereditary diseases often characterized by muscle weakness leading to physical motor impairment that ranges from mild to life-threatening disabilities (North, 2008). Several of these myopathies, including myotubular/centronuclear myopathies (CNM) and other myopathies with congenital fibre size disproportion, demonstrate early myofibre hypotrophy (Jungbluth et al., 2008; North, 2008; Romero, 2010). However, the underlying pathogenic mechanisms remain largely unknown.

In dogs and humans, *HACD1 (3-hydroxyacyl-CoA dehydratase 1)* deficiency has been associated with recessive congenital myopathies characterized by early-onset muscle weakness (Muhammad et al., 2013; Pelé et al., 2005). Early postnatal heterogeneity in myofibre size has been reported in both species, whereas progressive nuclear centralization has been observed in diseased dogs, a hallmark of CNM (Tiret et al., 2003). *HACD1* encodes an endoplasmic reticulum (ER)-resident enzyme that interacts with ELOVL1-7, KAR and TER proteins to form a complex involved in the synthesis of very long chain fatty acids (VLCFAs) (Ikeda et al., 2008; Ohno et al., 2010). As opposed to fatty acids up to C16, synthesized by a cytosolic fatty acid synthase, the longer VLCFAs are elongated within the ER in a four-step cycle (Kihara, 2012). In mammals, four paralogous genes encoding HACD1-4 catalyze the third step of this elongation cycle (Ikeda et al., 2008).

Following their incorporation into membrane lipids (such as phospholipids and sphingolipids), VLCFAs elicit specific functions based on their chain length and degree of unsaturation (Guillou et al., 2010; Kihara, 2012). In particular, they promote strong membrane curvature and vesicle fusion (Molino et al., 2014; Schneiter et al., 2004). In yeast, VLCFA elongation complex displays physical interactions with the desaturase enzyme that catalyzes the unsaturation of fatty acids (Miller et al., 2005), indicating interconnections between pathways involved in lipid balance. Although *Hacd1* deficiency was reported to impair myoblast growth and differentiation *in vitro* (Lin et al., 2012), no molecular role for HACD1 has yet been reported in muscle cells.

We hypothesized that heterogeneity of muscle fibre size in *HACD1*-related myopathies reflects a defect in muscle fibre development, due to altered lipid balance. Muscle fibre development occurs from embryogenesis through the early postnatal development and can be recapitulated in adults following muscle injury. During myofibre development, mononucleated precursor cells, called myoblasts, differentiate through a well-defined process

(Buckingham, 2001; Bentzinger et al., 2012). Myoblasts are derived from embryonic precursors or adult muscle satellite stem cells and once activated, are committed to a myogenic program via a cascade of transcription factor activation that triggers myoblast fusion, leading to the formation of large, multinucleated myofibres able to generate contractile force. A wealth of accumulated *in vivo* data strongly suggests that myoblast fusion is a limiting step for optimal myofibre growth, muscle mass and regenerative capacity (Horsley et al., 2001; Doherty et al., 2005; Georgiadis et al., 2007; Laurin et al., 2008; Hochreiter-Hufford et al., 2013; Millay et al., 2013; Lenhart et al., 2014; Millay et al., 2014). Similar to other processes involving membrane fusion (Chernomordik and Kozlov, 2005), myoblast fusion is the result of a complex interplay between lipids and proteins, which specific roles are just now being unraveled (Abmayr and Pavlath, 2012; Aguilar et al., 2013). A drop in membrane rigidity, known to promote membrane fusion in other cellular contexts (Maxfield and Tabas, 2005), is observed just before myoblast fusion (Prives and Shinitzky, 1977), and modifications in membrane lipid composition, putatively yielding a raise in membrane fluidity, have been reported during myoblast differentiation (Nakanishi et al., 2001; Briolay et al., 2013). Giving further support that lipids have an important role in regulating membrane fusion, adding unsaturated fatty acids to the culture media that purportedly increase membrane fluidity increases the capacity of myoblasts to fuse (Prives and Shinitzky, 1977; Nakanishi et al., 2001; Lee et al., 2009; Briolay et al., 2013). In contrast, lysophosphatidylcholine, which inhibits lipid bilayer fusion due to its inverted cone shape (Chernomordik and Kozlov, 2005), prevents myoblast fusion when added to culture media (Leikina et al., 2013). Altogether, these data suggest a model where naturally occurring modifications of the lipid membrane composition and concomitant alterations in fluidity would play key role in myoblast fusion. However, little is known regarding the genetic control of these modifications; in addition, the physiological and clinical relevance of modifications in composition and fluidity of myoblast membrane has yet to be investigated.

Given the enzymatic function of HACD1 and its implication in muscle homeostasis, we decided to address its precise role in muscle fibre development in the light of its molecular properties. We investigated this role by using combined *in vitro* and *in vivo* experiments in mice and dogs.

Results

HACD1 is required for muscle fibre growth

HACD1 loss-of-function mutations have been associated with congenital myopathies in humans and dogs (Pelé et al., 2005; Muhammad et al., 2013). To confirm the causative role of HACD1 deficiency in skeletal muscle impairment, we generated *Hacd1*-knockout mice using a recombinant null allele inserting the *LacZ* reporter gene (Supplementary Figure 1A-C). Heterozygous mice for the knockout allele were morphologically and histologically indistinguishable from their wild type littermates, in accordance with the recessive inheritance pattern of *HACD1* mutation in human and dog (Pelé et al., 2005; Muhammad et al., 2013); they were used alongside wild type mice as controls. In contrast, homozygous mice for the knockout allele (hereafter $Hacd1^{-/-}$ mice), although viable and fertile, presented a reduced body weight gain after birth (Figure 1A). At one week of age, body weight of $Hacd1^{-/-}$ mice was reduced by 14.6% compared to control mice ($P < 0.01$). The reduced weight gain was never compensated in adulthood despite a normal body size (Supplementary Figure 1D), with a 15.2% and a 16.4% reduction in body weight at 12 wk and 6 mo of age compared to control mice, respectively ($P < 0.05$ and 0.01, respectively). This reduction in body weight could be more specifically attributed to a 29% reduction in muscle weight (Figure 1B and C) and correlated with a 27.5% reduction in the muscle absolute maximal force compared to controls (Figure 1D), however leaving specific maximal force unchanged (Supplementary Figure 1E). In accordance with a deleterious muscle weakness, $Hacd1^{-/-}$ mice often displayed kyphosis (Supplementary Figure 1F).

This phenotype was reminiscent of that of *HACD1*-deficient Labrador retrievers (hereafter $HACD1^{cnm/cnm}$ or CNM dogs; (Tiret et al., 2003; Maurer et al., 2012)). As for $Hacd1^{-/-}$ mice, CNM dogs had reduced weight gain in the first weeks of life compared with controls (Supplementary Figure 2A). Postural and locomotor weakness was obvious between 2 and 6 mo of age and histological analyses of skeletal muscles from 5-mo-old CNM-affected pups revealed that amyotrophy was accompanied by heterogeneity in muscle fibre diameter (Figure 2A and B). Comparative studies between CNM dogs and $Hacd1^{-/-}$ mice (Figure 2A,B and E,F) revealed that in both cases, the mean myofibre diameter was reduced by 29.7 and 22.3% respectively (Figure 2C and 2G) and the distribution of fibre diameters was shifted towards smaller diameters in comparison with controls (Figure 2D and 2H); in $Hacd1^{-/-}$ mice, the number of myofibres per muscle was unchanged (Figure 2I), indicating that fibre hypotrophy *per se* yielded the reduced muscle mass.

These data suggested an early requirement of *HACD1* during muscle development and an important role for muscle fibre growth.

Hacd1 is required for optimal myoblast fusion

In order to characterize the cause of the reduced muscle mass and further discriminate between muscle atrophy and hypotrophy, we recapitulated myofibre development during muscle regeneration in both dogs and mice. The course of regeneration was similar in controls, CNM dogs and *Hacd1*$^{-/-}$ mice. Four to 6 days after notexin-induced injury, massive muscle necrosis and cellular infiltration were observed (Supplementary Figure 1G and 2C), replaced at Day 15 by regenerating myofibres (Figure 3A, B, D, E, G, H and Supplementary Figure 2C). However, newly formed myofibres were already significantly hypotrophic and the largest myofibres were almost completely absent in CNM dogs and *Hacd1*$^{-/-}$ mice (Figure 3C, F, I and J), identifying myofibre hypotrophy as a pathogenic mechanism. This reduced diameter of fibres was still present at Days 30 and 90 of regeneration in CNM dogs (Supplementary Figure 2C), indicating that no compensatory growth overcame this developmental defect. It is well-accepted that a deficit in muscle fibre growth observed at this stage of regeneration results from a defect in myoblast fusion (Horsley et al., 2001; Doherty et al., 2005; Georgiadis et al., 2007; Hochreiter-Hufford et al., 2013; Lenhart et al., 2014; Millay et al., 2014). Accordingly, nuclear counts at Day 15 confirmed that myofibres containing two nuclei were over-represented in *Hacd1*$^{-/-}$ mice compared to controls, whereas myofibres with 7 nuclei (the highest number counted at this stage) were depleted (Figure 3K).

To further confirm the impairment of myoblast fusion and determine if this defect was combined with a depletion in satellite cells, we first assessed in mice muscles the number of *Pax7*-positive satellite cells from which myoblasts differentiate to form new myofibres. Both immunofluorescence and RT-qPCR experiments indicated a similar expression of *Pax7* in *Hacd1*$^{-/-}$ mice compared to controls (Supplementary Figure 3A-D), excluding reduced numbers of satellite cells as causative of hypotrophy. We then used the capacity of primary myoblasts isolated from young pups to differentiate *in vitro* to characterize the contribution of *Hacd1* in fusion. After 2 days of differentiation, cells isolated from control and *Hacd1*$^{-/-}$ pups similarly formed myotubes and the number of nuclei within Myosin Heavy Chain-positive cells was similar, indicating normal myoblast commitment into the differentiation process (Figure 4A-C). In contrast, myotubes were globally smaller in cultures from *Hacd1*$^{-/-}$ pups and presented a reduced fusion index assessed by the average number of nuclei per myotube (Figure 4A, B and D). Accordingly, distribution of myotubes with respect to their number of

nuclei revealed fewer myotubes with ≥ 6 nuclei, and greater numbers of small myotubes with only 2 nuclei compared with controls (Figure 4E).

Together, these results demonstrate that both in dogs and mice, *Hacd1* function triggers the optimal fusion of myoblasts during their differentiation, sustaining the normal growth of muscle fibres within muscles.

The muscle-enriched *Hacd1-fl* isoform is upregulated during muscle development and regeneration

During embryogenesis of *Hacd1*$^{+/-}$ mice, strong expression of the *LacZ* reporter gene was observed in heart and skeletal muscle precursors (Figure 5A). *LacZ* expression was also highly induced in adult skeletal muscles during injury-induced regeneration (Figure 5B) and, more precisely, in regenerating myofibres recognizable by the alignment of central nuclei (Figure 5C).

In wild type dogs, two *HACD1* splice variants are expressed in normal skeletal muscles: the *HACD1-fl* full-length isoform retains the seven exons of the gene whilst the *HACD1-d5* isoform lacking exon 5 encodes a truncated protein (Pelé et al., 2005). RT-PCR conditions designed to amplify both variants revealed a broad expression of the *Hacd1-d5* isoform in mouse tissues (Figure 5D). In contrast, *Hacd1-fl* expression was nearly restricted to the heart and skeletal muscles, and in these tissues it was the predominant, highly-expressed isoform. During mouse embryonic development, a shift in *Hacd1* splicing occurred between day 7 and 17, with a marked increase in *Hacd1-fl* expression at the expense of *Hacd1-d5* (Figure 5D). This embryonic period spans muscle fibre maturation (Buckingham, 2001). To evaluate whether these two variants would play specific dynamic roles during muscle growth, we investigated by RT-(q)PCR their temporal expression during *in vitro* differentiation of wild type mouse primary or normal C2C12 myoblasts. We observed that formation of myotubes followed a marked upregulation of *Hacd1-fl* expression whereas *Hacd1-d5* expression was only mildly increased or did not change in both primary myoblasts (Figure 5E,F) and C2C12 (Figure 5G,H). *In vivo*, *Hacd1* was also markedly induced during muscle regeneration, strengthening *Hacd1-fl* predominance over *Hacd1-d5* in muscles (Figure 5I). Expression of *Hacd2* and *Hacd3* did not change during differentiation (Supplementary Figure 3E).

HACD1-FL is necessary for myoblast fusion

HACD1-FL protein is a vertebrate ortholog of the yeast enzyme Phs1 and displays HACD activity (Ikeda et al., 2008). In addition, we reported above a broad expression of *Hacd1-d5* in mouse tissues; besides, *HACD1-167*, an aberrant splice variant retaining exons 1, 6 and 7, specifically accumulated in muscles from CNM dogs (Pelé et al., 2005). We thus investigated

whether the two HACD1-D5 and HACD1-167 proteins encoded by these isoforms, predicted respectively to exhibit two or three transmembrane domains instead of the six identified in HACD1-FL (Supplementary Figure 4A), shared cellular and molecular features with HACD1-FL. In myogenic cells, all three isoforms correctly localized to the ER. In addition, HACD1-FL, HACD1-D5, HACD1-167, as well as HACD2, HACD3 and HACD4 physically interacted with all other proteins of the elongation complex, with the exception of HACD1-D5 that did not interact with TER (Supplementary Figure 4B-D). *In vitro*, enzymatic assays revealed that HACD1-FL, but neither HACD1-D5 nor HACD1-167, catalyzed the dehydration of 3-hydroxypalmitoyl-CoA into 2,3-*trans*-hexadecenoyl-CoA, in a dose-dependent manner (Figure 6A and Supplementary Figure 4E). Accordingly, *in vivo* expression of HACD1-FL, but not HACD1-D5, HACD1-167 or HACD1-FL-Y171A in which the Y171 essential residue (Kihara et al., 2008) had been mutated, rescued cell growth arrest of *PHS1*-shutdown yeasts (Figure 6B and Supplementary Figure 4F).

To decipher the relative functional importance of HACD1 isoforms during muscle cell differentiation, we stably knocked down *Hacd1* expression in C2C12 cells using a small hairpin interfering RNA targeting the wild type *Hacd1-fl* and *Hacd1-d5* isoforms (Supplementary Figure 5A). Myotube formation was severely impaired in *Hacd1*-knocked down (sh-*Hacd1)* cells (Figure 6C), confirming previous data (Lin et al., 2012). Defective fusion events were highlighted by a severe reduction in the number of nuclei per sh-*Hacd1* myotube, compared to controls (Figure 6C and D), although commitment of sh-*Hacd1* cells into the differentiation process was confirmed by increased expression of the *Myogenin* and *Myosin, heavy polypeptide 2, skeletal muscle, adult (Myh2)* myogenic markers (Supplementary Figure 5B-D) in line with the phenotype of the *Hacd1*$^{-/-}$ myoblasts (Figure 4A and B). This phenotype was thus consistent with our *in vivo* experiments that revealed an impairment in myoblast fusion upon HACD1 deficiency.

To evaluate the function of each isoform, we transduced sh-*Hacd1* cells with retroviral vectors driving the expression of shRNA-insensitive sequences encoding each of them (sh-*Hacd1*+*isoform* cells) (Supplementary Figure 5E and F). Importantly, rescue of the fusion impairment could be elicited only when the catalytically active HACD1-FL isoform was expressed, demonstrating the essential role of its specific activity in myoblast fusion (Figure 6C and D).

In parallel, *sh-Hacd1* cells exhibited a reduced proliferation rate (data not shown), as previously reported with the same interfering sequence (Lin et al., 2012). However, in our hand, this phenotype was neither rescued by HACD1-FL nor by HACD1-D5 and hence likely resulted from an off-target effect of the RNA interference. The fact that HACD1-FL could

rescue the fusion defect without rescuing the proliferation defect further indicates that the proliferation rate did not interfere with the fusion capacity of sh-*Hacd1* cells.

HACD1-FL regulates lipid balance and membrane fluidity

To identify the putative HACD-dependent changes in lipid content during myoblast differentiation, we compared phospholipid fatty acid contents in proliferative C2C12 myoblasts, when the *Hacd1-fl* to *Hacd1-d5* ratio was the lowest, with those at Day 3 of differentiation, corresponding to one day after the peak of *Hacd1-fl* expression (Figure 5G,H and Supplementary Figure 3E).

As lysophosphatidylcholine (LPC) acts as a potent inhibitor of myoblast fusion when added to the differentiation medium (Leikina et al., 2013), we first evaluated whether the relative content of phospholipid species would be modified upon *Hacd1* modulation (Supplementary Table 2). In control myoblasts, differentiation was accompanied by a nearly two-fold drop in LPC that was abolished in sh-*Hacd1* myoblasts and fully restored in sh-*Hacd1*+FL cells (Figure 7A and Supplementary Table 2A). This global dynamic profile was underlain by the individual profile of most LPCs (Supplementary Table 2B). This result demonstrated that HACD1-FL activity is responsible for the drop in LPC content preceding fusion. Myoblast differentiation was also accompanied by an increase in the level of phosphatidylinositols and a decrease in lysophosphatidylethanolamines that were independent of *Hacd1* expression (Supplementary Table 2A).

In parallel, we evaluated fatty acid content in the whole phospholipid pool (Supplementary Table 3). As C18 species are the smallest fatty acids produced by the VLCFA elongation complex (Ohno et al., 2010), the ratio of C18-C26/C10-C16 fatty acids reflected the elongation efficiency. Compared to controls, the ratio was decreased in sh-*Hacd1* cells both in proliferation and in differentiation, and this elongation defect was alleviated by HACD1-FL re-expression whereas it was amplified following HACD1-D5 expression (Figure 7B and Supplementary Table 3A and B). These results confirmed a positive role of HACD1-FL in the elongation of ≥C18 fatty acids and revealed an antagonistic role for HACD1-D5. Accordingly, the increase in the *Hacd1-fl* to *Hacd1-d5* ratio reported above in differentiating control myoblasts was accompanied by an increase in the C18-C26/C10-C16 ratio (Figure 7B and Supplementary Table 3B).

Interactions between the yeast desaturase Ole1 and the VLCFA elongation complex have been described (Miller et al., 2005). To evaluate whether such an interaction could be conserved and functional in mammals, we investigated the saturation status of phospholipid fatty acids in myoblasts. Indeed differentiating sh-*Hacd1* myoblasts had an increased

saturated fatty acid (SFA) content, at the expense of monounsaturated fatty acids (MUFA) (Figure 7C and Supplementary Table 3C). Re-expression of HACD1-FL fully restored normal SFA and MUFA contents and slightly increased the polyunsaturated fatty acid (PUFA) content. During proliferation too, HACD1-FL promoted MUFA accumulation at the expense of SFA and HACD1-D5 isoform exhibited an antagonist role (Supplementary Figure 6A and Supplementary Table 3C).

Unsaturation of fatty acids contained in phospholipids is known to increase fluidity of lipid bilayers (Maxfield and Tabas, 2005). To check whether the altered contents of SFA, MUFA and PUFA could have a functional impact on myoblasts, we analyzed their plasma membrane fluidity at Day 3 of differentiation and found that it was reduced by 9% in sh-*Hacd1* cells at 37°C ($P = 5.10^{-5}$). Fluidity was fully restored by HACD1-FL re-expression (Figure 7D and Supplementary Figure 6B).

Discussion

We showed that HACD1-deficient mice and dogs exhibit an early-onset hypotrophy of myofibres that could be recapitulated during muscle regeneration after injury, two characteristics of myoblast fusion impairment (Horsley et al., 2001; Doherty et al., 2005; Georgiadis et al., 2007; Laurin et al., 2008; Hochreiter-Hufford et al., 2013; Millay et al., 2013; Lenhart et al., 2014; Millay et al., 2014). Defective myoblast fusion upon HACD1 deficiency was confirmed both *in vivo* and *in vitro*, as indicated by smaller myofibres containing fewer nuclei. Such an early phenotype could be the result of a defect either in myoblast differentiation or in myoblast fusion *per se*. On the contrary to previously published data (Lin et al., 2012), we observed a normal commitment of both primary myoblasts and C2C12 cells into the differentiation upon *Hacd1* deficiency; in both cases, we reproducibly showed at the RNA and protein levels that *Hacd1* deficiency neither impaired *Myogenin* and *Myh2* expression nor reduced the proportion of cells positive for MHC, a marker of terminal differentiation. This demonstrates that myoblast fusion step was more specifically affected by *Hacd1* deficiency.

On the molecular level, we showed that during myoblast differentiation, HACD1-FL activity prompts a drop in the content of LPC, an inhibitor of myoblast fusion (Leikina et al., 2013). In parallel, it promoted a slight increase in ≥C18 fatty acids, a rise in MUFA content and a drop in plasma membrane rigidity. We propose a model in which HACD1-FL upregulation during myoblast differentiation modifies membrane lipid balance and its physical properties to promote efficient fusion, eventually leading to optimal muscle mass and force (Figure 7E).

In CNM dogs (Pelé et al., 2005), exchange of wild type *HACD1* transcripts by those of the *HACD1-167* isoform (which encodes an inactive protein), mimics the human condition in which a non-sense mutation abrogates the HACD activity of the encoded protein (Muhammad et al., 2013). As the presence of small myofibres is also observed in HACD1-deficient humans, we suggest that defective myoblast fusion constitutes a novel, non-exclusive pathological mechanism that participates to the reduction in muscle mass and strength observed upon HACD1 deficiency. More generally, myofibre heterogeneity with hypotrophic fibres is an early feature of other myopathies with congenital fibre size disproportion and CNM/MTM myopathies (Jungbluth et al., 2008; North, 2008; Nance et al., 2012). Importantly, small fibre diameter, but not the proportion of central nuclei, is associated with the most severe *MTM1* mutations and constitutes the worst outcome in myotubular patients (Pierson et al., 2007). Hence we propose that defective myoblast fusion might constitute a synergistic pathogenic mechanism operating in these congenital myopathies (Ravenscroft et

al., 2014). If confirmed, a fusion defect would have direct medical consequences, as it will be mandatory to envisage its early correction within the very first period of postnatal life. Additional mechanisms underlying the accompanying concomitant development of hypertrophic fibres in some cases of myopathies with congenital fibre size disproportion (Jungbluth et al., 2008; Muhammad et al., 2013), would also need to be assessed. Importantly, no major cardiovascular phenotype could be observed in HACD1-deficient young adult dogs and mice, which heart and cardiovascular parameters were thoroughly evaluated using electrocardiography, arterial blood pressure measurement, echocardiography and tissue-doppler imaging (data not shown). Of note, in contrast to skeletal muscles, heart development does not rely on cell fusion events. This developmental difference may contribute to protecting the heart from morbid consequences of HACD1-deficiency; it also highlights the pathogenic role of fusion impairment in skeletal muscles.

Changes in membrane fluidity and the degree of saturation of membrane fatty acids each influence myoblast fusion (Prives and Shinitzky, 1977; Nakanishi et al., 2001; Briolay et al., 2013). Our results emphasize that *Hacd1* may play a pivotal role in the integrated genetic control of these previously reported changes, as well as in the newly identified drop in LPC level. During myofiber development, *Hacd1-fl* is upregulated and counteracts the *Hacd1-d5* ubiquitous isoform that exerts an antagonistic role through a still unknown mechanism. As a direct consequence of its 3-hydroxyacyl-CoA dehydratase activity in the VLCFA elongation complex (Ikeda et al., 2008), HACD1-FL promoted an increase in the C18-C26 to C10-C16 ratio during myoblast differentiation. Our data also revealed indirect key functions of *Hacd1* that were not predicted by its HACD activity, which consist in an increased MUFA content at the expense of SFA content and in a drop in both membrane rigidity and LPC content. While there are growing evidences of structural and functional interactions between enzymes of different lipid pathways that we did not investigate in this study, our results suggest a significant interplay of these pathways during myoblast fusion and indicate that *Hacd1* plays a key role in their integrated regulation. These results also open novel medical avenues, as manipulation of the complex *Hacd1*-dependent lipid balance may represent an alternative, non-invasive therapeutic strategy in *HACD1*-related or other congenital myopathies.

Although these changes might influence different steps of myoblast fusion such as myoblast migration or membrane merging, they are all expected to favor membrane fusion *per se*. First, LPC has been reported to inhibit several events of membrane fusion (Reporter and Raveed, 1973; Chernomordik et al., 1993; Yeagle et al., 1994; Ciechonska and Duncan, 2014), presumably because its inverted cone-shape interferes with the negative membrane curvature required for the hemifusion step (Chernomordik and Kozlov, 2005). Accordingly, LPC can

reversibly inhibit myoblast fusion, although its effect may depend upon its concentration and the stage of fusion (Leikina et al., 2013; Teng et al., 2015). Our data showed that *Hacd1* regulates the LPC drop normally observed during myoblast differentiation. We suggest that this drop in total membranes increases myoblast permissiveness to fusion and that the failure of this drop observed in *Hacd1*-deficient cells constitutes a major determinant of myoblast fusion impairment in HACD1-deficient conditions. Whether this LPC drop is of significant importance for specific membrane compartments, including the plasma membrane, will require further analyses. In parallel, longer acyl chains of VLCFAs are proposed to fill the voids created during membrane bending and to stabilize strong membrane curvatures (Schneiter et al., 2004; Chernomordik and Kozlov, 2005). Like other fusion processes, myoblast fusion involves a hemifusion stage for plasma membranes, during which lipids from the two merging outer layers are mixed (Chernomordik and Kozlov, 2005; Leikina et al., 2013), followed by the formation of a fusion pore inducing cell content mixing. These two sequential steps necessitate strong membrane curvature that would be favored by VLCFAs, in accordance with the defective vesicle fusion observed during cytokinesis in plants lacking VLCFA-containing sphingolipids (Molino et al., 2014). Finally, membrane fluidity is a well-known determinant of successful membrane fusion (Maxfield and Tabas, 2005) and in myoblasts, it could also promote fusion by concentrating fusion-associated factors or lipid rafts at sites of contact between activated myoblasts (Abmayr and Pavlath, 2012). During myoblast differentiation, we showed that *Hacd1* activation yields increased levels of MUFAs at the expense of SFAs, a mechanism that likely participates to the increased membrane fluidity and would explain the enhanced myoblast fusion reported following addition of unsaturated fatty acids, whereas saturated fatty acids or cholesterol, a membrane rigidifier, tend to inhibit fusion (Prives and Shinitzky, 1977; Nakanishi et al., 2001; Lee et al., 2009; Briolay et al., 2013).

In conclusion, the results presented here provide a unifying genetic control accounting for several changes in lipid balance that likely confer permissiveness for myoblast fusion in an additive manner. This promoting function would result from the increase in *Hacd1-fl* expression following a muscle-enriched splicing mechanism. In addition to increasing the VLCFA content through its HACD enzymatic activity, HACD1-FL would modify MUFA and LPC levels indirectly, by regulating their respective biosynthetic pathways. Desaturation of SFAs into MUFAs mostly relies on the desaturase activity of ER-resident stearoyl-CoA desaturase proteins (Guillou et al., 2010), and in yeast, physical interactions described between the desaturase Ole1 and proteins of the VLCFA elongation complex (Miller et al., 2005) suggest functional cross-talk between the two enzymatic pathways. The LPC level

results from a more complex mechanism since it can be generated either by the cleavage of phosphatidylcholine by phospholipase A2 or by the lecithin-cholesterol acyl-transferase activity. Interestingly, it has been shown that increased LPC synthesis constitutes an important step leading to atherosclerosis (Schmitz and Ruebsaamen, 2010). LPC is also released by several tumor cell lines and because of autotaxin activity, generates the potent cell motility activator lysophosphatidic acid (Gotoh et al., 2012). Thus, identification of splicing factors that upregulate *Hacd1-fl* and reduce LPC expression, which is an issue in developmental myology, might be of wider medical interest.

Further studies will be required to precisely assess the role of *Hacd1* on the metabolism, subcellular localization and function of these candidate lipids, as well as on the indirect modulation of pathways regulating LPC and unsaturated fatty acids contents.

Materials and Methods

Mice and myoblasts

The *Hacd1* knockout recombination vector (PRPGS00067_A_B09) was obtained from the Knockout Mouse Project Repository (KOMP; https://www.komp.org) and was electroporated into C57BL/6N ES cells. All experiments were performed on mice generated from two independent ES clones. Matings between *Hacd1*$^{+/-}$ mice generated control (wild type and *Hacd1*$^{+/-}$) and *Hacd1* knockout (*Hacd1*$^{-/-}$) mice for all the described experiments.

The ANSES/EnvA/Upec Ethics Committee (C2EA – 16; www.enseignementsup-recherche.gouv.fr) approved the experiments performed on mice (approval numbers 11/11/15-2 and 20/12/12-16).

sh-*Hacd1* and control myoblasts were obtained by selecting puromycin-resistant clones of C2C12 myoblasts, respectively transfected with two different shRNA pGIPZ lentiviral vectors against *Hacd1* exon 4 or a control vector (OpenBiosystems).

Statistical analysis

A t-test-ANOVA with repeated measure factor was applied to paired data, i.e. in the case of measurement of fibre number, size, nuclear content or PAX7-positive cell content on muscle sections, as well as mass measurements of paired muscles in mice. Student T test was used for all other analyses and Welch modification was applied when sample number was low ($n < 4$). Data are expressed as mean ± standard error of the mean and differences were considered significative when $P < 0.05$.

Experimental details

Experimental details of regeneration experiments in dogs and mice; immunological and histological staining; muscle section analyses; tetanic force measurement; PCR, RT-PCR and RT-qPCR experiments; fluidity; HACD activity measurements; phospholipid analyses; co-affinity purification experiments; additional ethics statement are available in the Supplementary information file.

Acknowledgements

We thank the UETM team for daily care to the dogs; UC Davis and the NIH KOMP for *Hacd1* targeting vector; F. Langa-Vives (CIGM, Institut Pasteur) for generation of *Hacd1*-knockout mice; A. Athias, J.-P. Pais de Barros for lipid measurements and expertise (LAP platform) and DimaCell platform for membrane fluidity measurements (Dijon, France); H. Gaillot for his technical help; the animal facility of Necker (Paris) for providing *PGK-Cre* mice; O. Albagli for sharing MSCV plasmid; C.A Reynaud for access to facilities; L. Bessueille and M. Rialland for sharing technics; M. Pelé, J.-D. Faure and B. Payrastre for critical insights; M. Abitbol for statistical analysis; A. vandenBerg for editing the manuscript.

Funding

This work was supported by the Agence Nationale de la Recherche (ANR-12-JSV1-0005), the Association Française contre les Myopathies (14577, 15882 and 16143), the CNM Project (www.labradorcnm.com), the Alliance program (22866ZM), the Myotubular Trust and Grants-in-Aid for Scientific Research (B) to AK from Japan Society for the Promotion of Science (23370057). JB was supported by the French Ministry of Research and Technologies and the Université Paris 6 (Paris), VG and AR by the ANR, GW by the BBSRC CASE and the Myotubular Trust.

References

Abmayr, S.M., and Pavlath, G.K. (2012). Myoblast fusion: lessons from flies and mice. Development *139*, 641–656.

Aguilar, P.S., Baylies, M.K., Fleissner, A., et al. (2013). Genetic basis of cell–cell fusion mechanisms. Trends Genet. *29*, 427–437.

Bentzinger, C.F., Wang, Y.X., and Rudnicki, M.A. (2012). Building Muscle: Molecular Regulation of Myogenesis. Cold Spring Harb. Perspect. Biol. *4*, a008342.

Briolay, A., Jaafar, R., Nemoz, G., et al. (2013). Myogenic differentiation and lipid-raft composition of L6 skeletal muscle cells are modulated by PUFAs. Biochim. Biophys. Acta BBA - Biomembr. *1828*, 602–613.

Buckingham, M. (2001). Skeletal muscle formation in vertebrates. Curr. Opin. Genet. Dev. *11*, 440–448.

Chernomordik, L.V., and Kozlov, M.M. (2005). Membrane Hemifusion: Crossing a Chasm in Two Leaps. Cell *123*, 375–382.

Chernomordik, L.V., Vogel, S.S., Sokoloff, A., et al. (1993). Lysolipids reversibly inhibit Ca2+-, GTP- and pH-dependent fusion of biological membranes. FEBS Lett. *318*, 71–76.

Ciechonska, M., and Duncan, R. (2014). Lysophosphatidylcholine Reversibly Arrests Pore Expansion during Syncytium Formation Mediated by Diverse Viral Fusogens. J. Virol. *88*, 6528–6531.

Doherty, K.R., Cave, A., Davis, D.B., et al. (2005). Normal myoblast fusion requires myoferlin. Development *132*, 5565–5575.

Georgiadis, V., Stewart, H.J.S., Pollard, H.J., et al. (2007). Lack of galectin-1 results in defects in myoblast fusion and muscle regeneration. Dev. Dyn. *236*, 1014–1024.

Gotoh, M., Fujiwara, Y., Yue, J., et al. (2012). Controlling cancer through the autotaxin–lysophosphatidic acid receptor axis. Biochem. Soc. Trans. *40*, 31–36.

Guillou, H., Zadravec, D., Martin, P.G.P., et al. (2010). The key roles of elongases and desaturases in mammalian fatty acid metabolism: Insights from transgenic mice. Prog. Lipid Res. *49*, 186–199.

Hochreiter-Hufford, A.E., Lee, C.S., Kinchen, J.M., et al. (2013). Phosphatidylserine receptor BAI1 and apoptotic cells as new promoters of myoblast fusion. Nature *497*, 263–267.

Horsley, V., Friday, B.B., Matteson, S., et al. (2001). Regulation of the Growth of Multinucleated Muscle Cells by an Nfatc2-Dependent Pathway. J. Cell Biol. *153*, 329–338.

Ikeda, M., Kanao, Y., Yamanaka, M., et al. (2008). Characterization of four mammalian 3-hydroxyacyl-CoA dehydratases involved in very long-chain fatty acid synthesis. FEBS Lett. *582*, 2435–2440.

Jungbluth, H., Wallgren-Pettersson, C., and Laporte, J. (2008). Centronuclear (myotubular) myopathy. Orphanet J. Rare Dis. *3*.

Kihara, A. (2012). Very long-chain fatty acids: elongation, physiology and related disorders. J. Biochem. (Tokyo) *152*, 387–395.

Kihara, A., Sakuraba, H., Ikeda, M., et al. (2008). Membrane topology and essential amino acid residues of Phs1, a 3-hydroxyacyl-CoA dehydratase involved in very long-chain fatty acid elongation. J. Biol. Chem. *283*, 11199–11209.

Laurin, M., Fradet, N., Blangy, A., et al. (2008). The atypical Rac activator Dock180 (Dock1) regulates myoblast fusion in vivo. Proc. Natl. Acad. Sci. *105*, 15446–15451.

Lee, J.-H., Tachibana, H., Morinaga, Y., et al. (2009). Modulation of proliferation and differentiation of C2C12 skeletal muscle cells by fatty acids. Life Sci. *84*, 415–420.

Leikina, E., Melikov, K., Sanyal, S., et al. (2013). Extracellular annexins and dynamin are important for sequential steps in myoblast fusion. J. Cell Biol. *200*, 109–123.

Lenhart, K.C., Becherer, A.L., Li, J., et al. (2014). GRAF1 promotes ferlin-dependent myoblast fusion. Dev. Biol. *393*, 298–311.

Lin, X., Yang, X., Li, Q., et al. (2012). Protein tyrosine phosphatase-like A regulates myoblast proliferation and differentiation through MyoG and the cell cycling signaling pathway. Mol. Cell. Biol. *32*, 297–308.

Maurer, M., Mary, J., Guillaud, L., et al. (2012). Centronuclear myopathy in Labrador retrievers: a recent founder futation in the PTPLA Gene has rapidly disseminated worldwide. PLOS ONE *7*, e46408.

Maxfield, F.R., and Tabas, I. (2005). Role of cholesterol and lipid organization in disease. Nature *438*, 612–621.

Millay, D.P., O'Rourke, J.R., Sutherland, L.B., et al. (2013). Myomaker is a membrane activator of myoblast fusion and muscle formation. Nature *499*, 301–305.

Millay, D.P., Sutherland, L.B., Bassel-Duby, R., et al. (2014). Myomaker is essential for muscle regeneration. Genes Dev. *28*, 1641–1646.

Miller, J.P., Lo, R.S., Ben-Hur, A., et al. (2005). Large-scale identification of yeast integral membrane protein interactions. Proc. Natl. Acad. Sci. U. S. A. *102*, 12123–12128.

Molino, D., Van der Giessen, E., Gissot, L., et al. (2014). Inhibition of very long acyl chain sphingolipid synthesis modifies membrane dynamics during plant cytokinesis. Biochim. Biophys. Acta BBA - Mol. Cell Biol. Lipids *1841*, 1422–1430.

Muhammad, E., Reish, O., Ohno, Y., et al. (2013). Congenital myopathy is caused by mutation of HACD1. Hum. Mol. Genet. *22*, 5229–5236.

Nakanishi, M., Hirayama, E., and Kim, J. (2001). Characterisation of myogenic cell membrane: II. Dynamic changes in membrane lipids during the differentiation of mouse C2 myoblast cells. Cell Biol. Int. *25*, 971–979.

Nance, J.R., Dowling, J.J., Gibbs, E.M., et al. (2012). Congenital Myopathies: An Update. Curr. Neurol. Neurosci. Rep. *12*, 165–174.

North, K. (2008). What's new in congenital myopathies? Neuromuscul Disord *18*, 433–442.

Ohno, Y., Suto, S., Yamanaka, M., et al. (2010). ELOVL1 production of C24 acyl-CoAs is linked to C24 sphingolipid synthesis. Proc. Natl. Acad. Sci. *107*, 18439–18444.

Pelé, M., Tiret, L., Kessler, J.-L., et al. (2005). SINE exonic insertion in the PTPLA gene leads to multiple splicing defects and segregates with the autosomal recessive centronuclear myopathy in dogs. Hum. Mol. Genet. *14*, 1417–1427.

Pierson, C.R., Agrawal, P.B., Blasko, J., et al. (2007). Myofiber size correlates with MTM1 mutation type and outcome in X-linked myotubular myopathy. Neuromuscul. Disord. *17*, 562–568.

Prives, J., and Shinitzky, M. (1977). Increased membrane fluidity precedes fusion of muscle cells. Nature *268*, 761–763.

Ravenscroft, G., Laing, N.G., and Bönnemann, C.G. (2014). Pathophysiological concepts in the congenital myopathies: blurring the boundaries, sharpening the focus. Brain awu368.

Reporter, M., and Raveed, D. (1973). Plasma membranes: isolation from naturally fused and lysolecithin-treated muscle cells. Science *181*, 863–865.

Romero, N.B. (2010). Centronuclear myopathies: A widening concept. Neuromuscul. Disord. *20*, 223–228.

Schmitz, G., and Ruebsaamen, K. (2010). Metabolism and atherogenic disease association of lysophosphatidylcholine. Atherosclerosis *208*, 10–18.

Schneiter, R., Brugger, B., Amann, C.M., et al. (2004). Identification and biophysical characterization of a very-long-chain-fatty-acid-substituted phosphatidylinositol in yeast subcellular membranes. Biochem J *381*, 941–949.

Teng, S., Stegner, D., Chen, Q., et al. (2015). Phospholipase D1 facilitates second-phase myoblast fusion and skeletal muscle regeneration. Mol. Biol. Cell *26*, 506–517.

Tiret, L., Blot, S., Kessler, J.-L., et al. (2003). The cnm locus, a canine homologue of human autosomal forms of centronuclear myopathy, maps to chromosome 2. Hum. Genet. *113*, 297–306.

Yeagle, P.L., Smith, F.T., Young, J.E., et al. (1994). Inhibition of membrane fusion by lysophosphatidylcholine. Biochemistry (Mosc.) *33*, 1820–1827.

Figure legends

Figure 1. Myopathy in *Hacd1*$^{-/-}$ mice.

(**A**) Weight gain in *Hacd1*$^{-/-}$, *Hacd1*$^{+/-}$ and wild type (WT) mice from birth to postanatal week three (n = 11, 15 and 12, respectively). (**B**) Photograph of *gastrocnemius* muscles from WT (left) and *Hacd1*$^{-/-}$ (right) 6-mo-old mice. (**C**) Mean mass of *gastrocnemius* and *tibialis anterior* (TA) muscles from 6-mo-old *Hacd1*$^{-/-}$, *Hacd1*$^{+/-}$ and WT mice (*gastrocnemius*: n = 5, 3 and 4 mice, respectively; TA: n = 9, 7 and 8 mice, respectively). (**D**) Mean absolute maximal force of TA muscles from *Hacd1*$^{-/-}$, *Hacd1*$^{+/-}$ and WT mice (n = 16, 12 and 16, respectively). Error bars correspond to standard error of the mean. *: $P < 0.05$; **: $P < 0.01$; ***: $P < 0.001$.

Figure 2. Defective myofibre growth in HACD1-deficient dogs and mice.

(**A** and **B**) H&E-stained transverse sections of *biceps femoris* muscles from 5-mo-old control (**A**) and *HACD1*$^{cnm/cnm}$ CNM-affected (**B**) dogs showing hypotrophic fibres in (**B**). (**C**) Average myofibre diameter (in μm) in 3- to 4-y-old control and *HACD1*$^{cnm/cnm}$ dogs (n = 3 for each genotype; ≥ 460 fibres examined per dog). (**D**) Percent distribution by diameter (μm) of myofibres analyzed in (**C**). (**E** and **F**) H&E-stained transverse sections of TA muscles from 3-mo-old control (*i.e.,* WT or *Hacd1*$^{+/-}$ (**E**)) and *Hacd1*$^{-/-}$ (**F**) mice showing fibre size disproportion in (**F**) (n = 3 for each condition). (**G**) Mean fibre diameter in TA muscles from 3-mo-old control and *Hacd1*$^{-/-}$ mice (n = 3 for each group; ≥ 780 fibres per mouse). (**H**) Percent distribution by diameter (μm) of myofibres analyzed in (**G**). (**I**) Mean number of total fibres in TA muscles from 3-mo-old control and *Hacd1*$^{-/-}$ mice (n = 5 for each group). Bars: 100 μm. Error bars correspond to standard error of the mean. *: $P < 0.05$; **: $P < 0.01$; ***: $P < 0.001$.

Figure 3. Defective myoblast fusion in HACD1-deficient dogs and mice.

H&E-staining of muscle transverse sections before (**A** and **B**) and at Day 15 after notexin injection (**D** and **E**) in control (**A** and **D**) and *HACD1*$^{cnm/cnm}$ (**B** and **E**) dogs. Bars: 200 μm. (**C** and **F**) Percent distribution by diameter (μm) of myofibres from dog muscles before (**C**) and at Day 15 after notexin injection (**F**) (n = 1 for each genotype; ≥ 730 fibres examined per dog). (**G** and **H**) Immunofluorescence for Dystrophin (green) on TA sections at Day 15 after notexin injection in control (**G**) and *Hacd1*$^{-/-}$ (**H**) mice. Nuclei are in blue. Bars: 100 μm. (**I**) Mean fibre diameter in TA muscles at Day 15 after notexin injection in control and *Hacd1*$^{-/-}$ mice (n = 3 and 4, respectively; ≥ 1780 fibres per mouse). (**J**) Percent distribution by diameter (μm) of myofibres analyzed in (**I**). (**K**) Nuclear content of fibres (n = 3 for each group; ≥ 600

fibres per mouse). Error bars correspond to standard error of the mean. *: $P < 0.05$; **: $P < 0.01$; ***: $P < 0.001$.

Figure 4. Defective myoblast fusion in normally differentiating HACD1-deficient myoblasts.

(**A** and **B**) Immunodetection on muscle primary cell cultures from control or *Hacd1*$^{-/-}$ newborns at Day 2 of differentiation of the Myosin Heavy Chains (MHC, green). Nuclei are in blue. Bars: 100 µm. (**C**) Unchanged differentiation index in HACD1-deficient myoblasts, *i.e.*, percentage of nuclei contained in MHC-positive cells (n = 5 for each newborn group; ≥ 1000 nuclei per sample). (**D**) Decreased fusion index in HACD1-deficient myoblasts, *i.e.*, average number of nuclei per myotube (n = 5 for each newborn group; ≥ 100 myotubes per sample). (**E**) Percent distribution of myotubes analyzed in (**D**) by their number of nuclei. Error bars correspond to standard error of the mean. *: $P < 0.05$; **: $P < 0.01$; ***: $P < 0.001$.

Figure 5. Upregulation of the muscle-specific, *Hacd1-full length* (*Hacd1-fl*) isoform during muscle fibre development.

(**A** and **B**) X-Gal staining of a *Hacd1*$^{+/-}$ embryo at E12.5 (**A**), TA muscles (**B**) from a *Hacd1*$^{-/-}$ mouse at Day 15 after injection of NaCl (left) or notexin (right). (**C**) Dissected fibres from the notexin-injected muscle shown in (**B**) showing X-Gal staining in a regenerative fibre (centralized nuclei, in blue). Bar: 20 µm. (**D**) RT-PCR experiments showing expression of *Hacd1* transcripts in mouse tissues and embryos. (**E** to **H**) Expression of *Hacd1* transcripts during differentiation of primary muscle cells (**E** and **F**) and C2C12 cells (**G** and **H**) revealed by RT-PCR experiments (**E** and **G**) or RT-qPCR experiments (**F** and **H**) showing fold-change from proliferation for each isoform (n = 3 for each condition). (**I**) RT-qPCR experiments for *Hacd1-fl* and *Hacd1-d5* isoforms in TA muscles from wild type mice, either non injected (n = 4) or at Day 6 (n = 3) or Day 15 (n = 4) after notexin injection. Error bars correspond to standard error of the mean. *: $P < 0.05$; **: $P < 0.01$; ***: $P < 0.001$.

Figure 6. Activity of HACD1 isoforms and role of *HACD1-fl* in myoblast fusion.

(**A**) Affinity-purified 3xFLAG-tagged HACD1 isoforms incubated with [^{14}C]3-hydroxypalmitoyl-CoA (3-OH FA) and separated by normal-phase thin layer chromatography. (**B**) Shutdown of *PHS1* in a yeast strain carrying *PHS1* under control of a tetracycline (doxycycline; DOX)-dependent promoter leads to a lethal phenotype, rescued only by the active wild type *HACD1-fl* isoform. Cells were serially diluted at 1:10. (**C**) At Day 5 of differentiation, sh-*Hacd1* cells failed to form elongated myotubes, a phenotype

rescued only by re-expression of the wild type *HACD1-fl* (sh-*Hacd1+fl*) isoform. Bars: 200 µm. (**D**) Fusion index of sh-*Hacd1* cells and sh-*Hacd1* cells re-expressing HACD1 isoforms (n = 3 for each condition).

Figure 7. HACD1 regulates lipid balance and membrane fluidity in myoblasts.

(**A**) Lysophosphatidylcholine (LPC) content, expressed as the percentage of total phospholipids, in proliferation and at Day 3 of differentiation. (**B**) Ratio of C18-26 to C10-16 phospholipid fatty acids in proliferation and at Day 3 of differentiation. (**C**) Proportions of saturated (SFA), monounsaturated (MUFA) or polyunsaturated (PUFA) fatty acids at Day 3 of differentiation. (**D**) Fluorescence anisotropy (*r*, inverse of fluidity) measured at Day 3 of differentiation. (**E**) Proposed model for the role of *Hacd1-fl* during muscle fibre development. Error bars correspond to standard error of the mean. *: $P < 0.05$; **: $P < 0.01$; ***: $P < 0.001$.

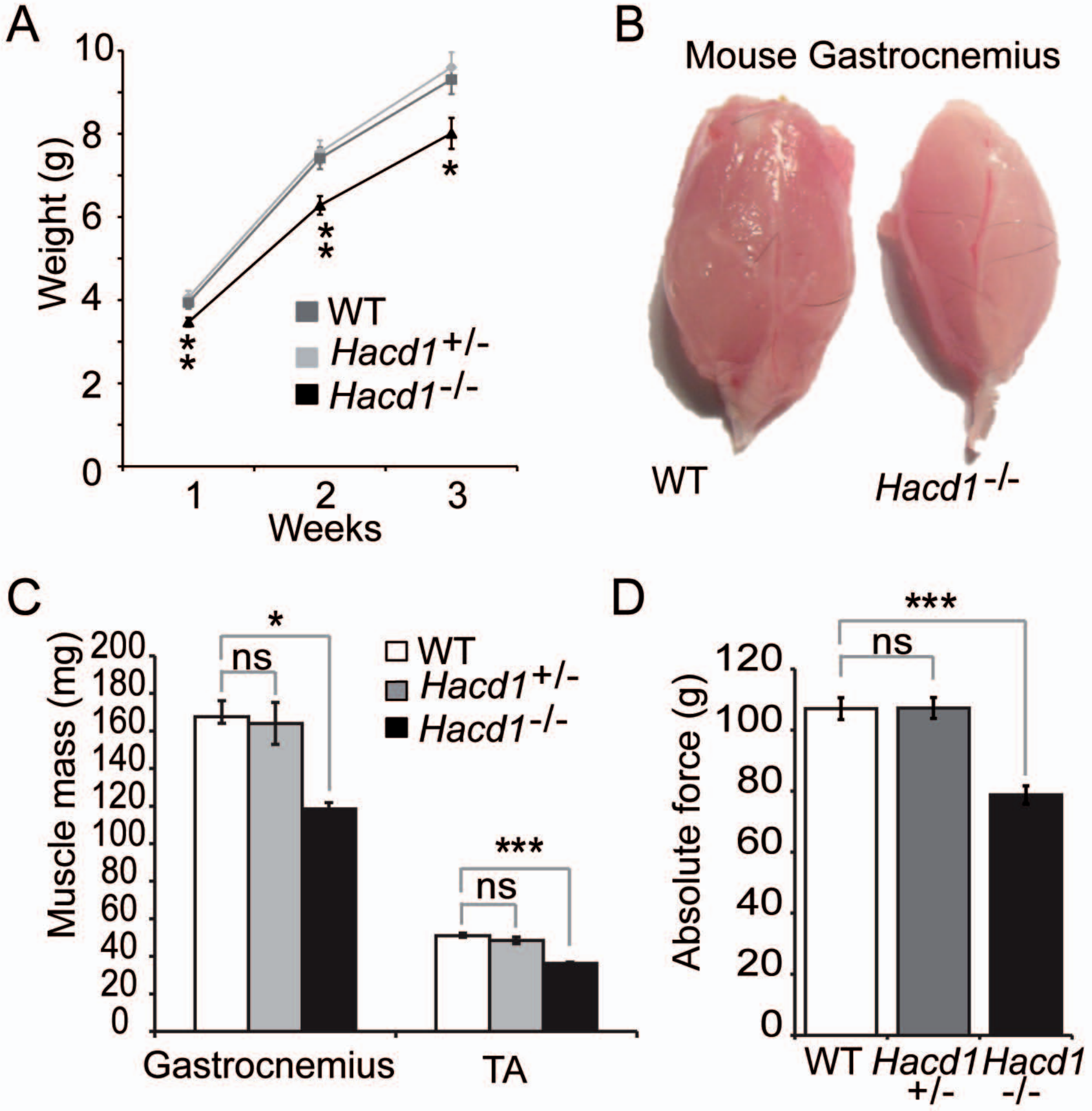
A
Weight (g)
10
8
6
4
2
0
1
2
3
Weeks
WT
Hacd1+/-
Hacd1-/-
**
**
*
B
Mouse Gastrocnemius
WT
Hacd1-/-
C
Muscle mass (mg)
200
180
160
140
120
100
80
60
40
20
0
*
ns
***
ns
WT
Hacd1+/-
Hacd1-/-
Gastrocnemius
TA
D
Absolute force (g)
120
100
80
60
40
20
0
***
ns
WT
Hacd1 +/-
Hacd1 -/-

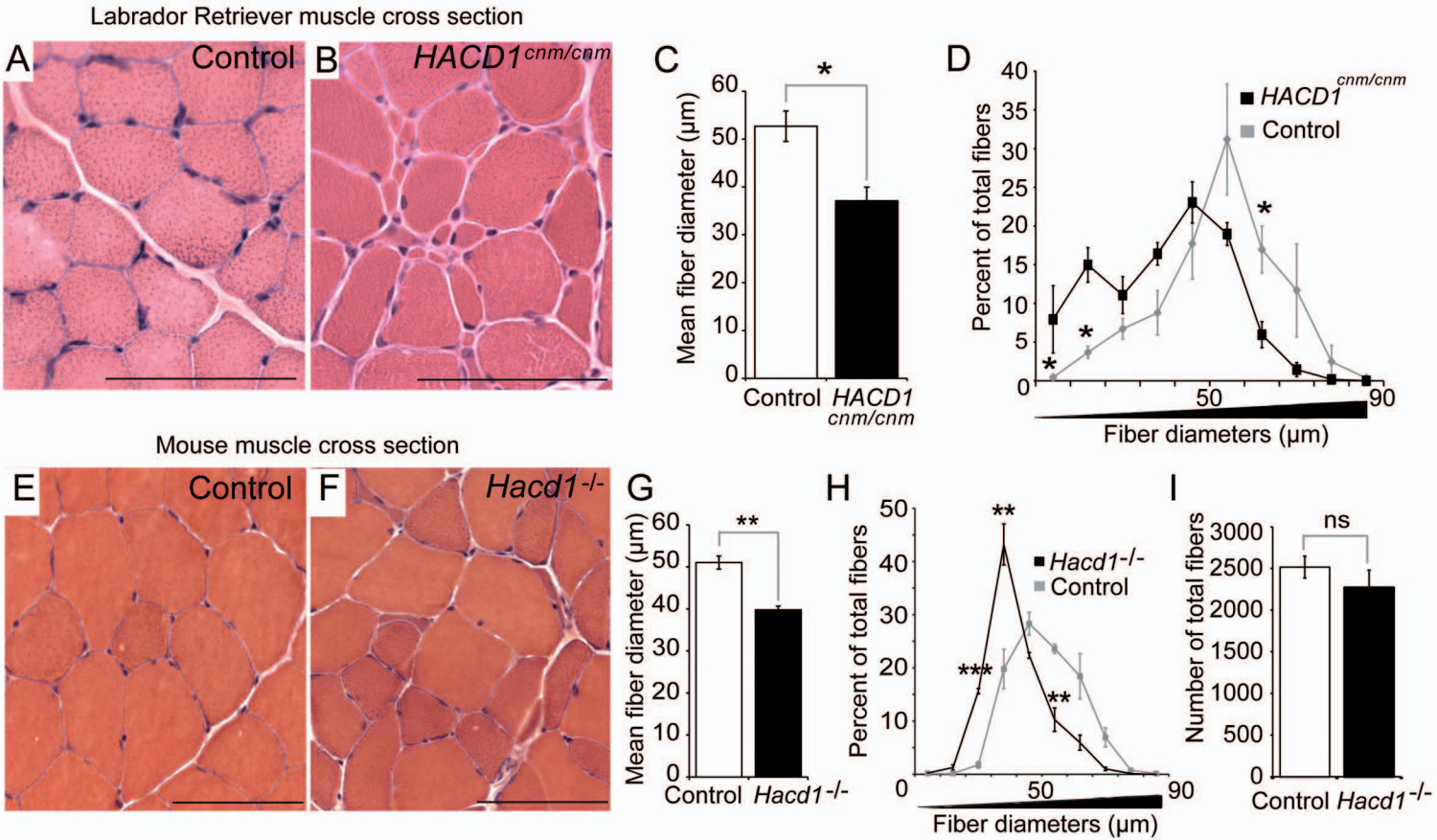
Labrador Retriever muscle cross section
A
Control
B
HACD1cnm/cnm
C
Mean fiber diameter (µm)
Control
HACD1 cnm/cnm
D
Percent of total fibers
HACD1cnm/cnm
Control
Fiber diameters (µm)
Mouse muscle cross section
E
Control
F
Hacd1-/-
G
Mean fiber diameter (µm)
Control
Hacd1-/-
H
Percent of total fibers
Hacd1-/-
Control
Fiber diameters (µm)
I
Number of total fibers
ns
Control
Hacd1-/-

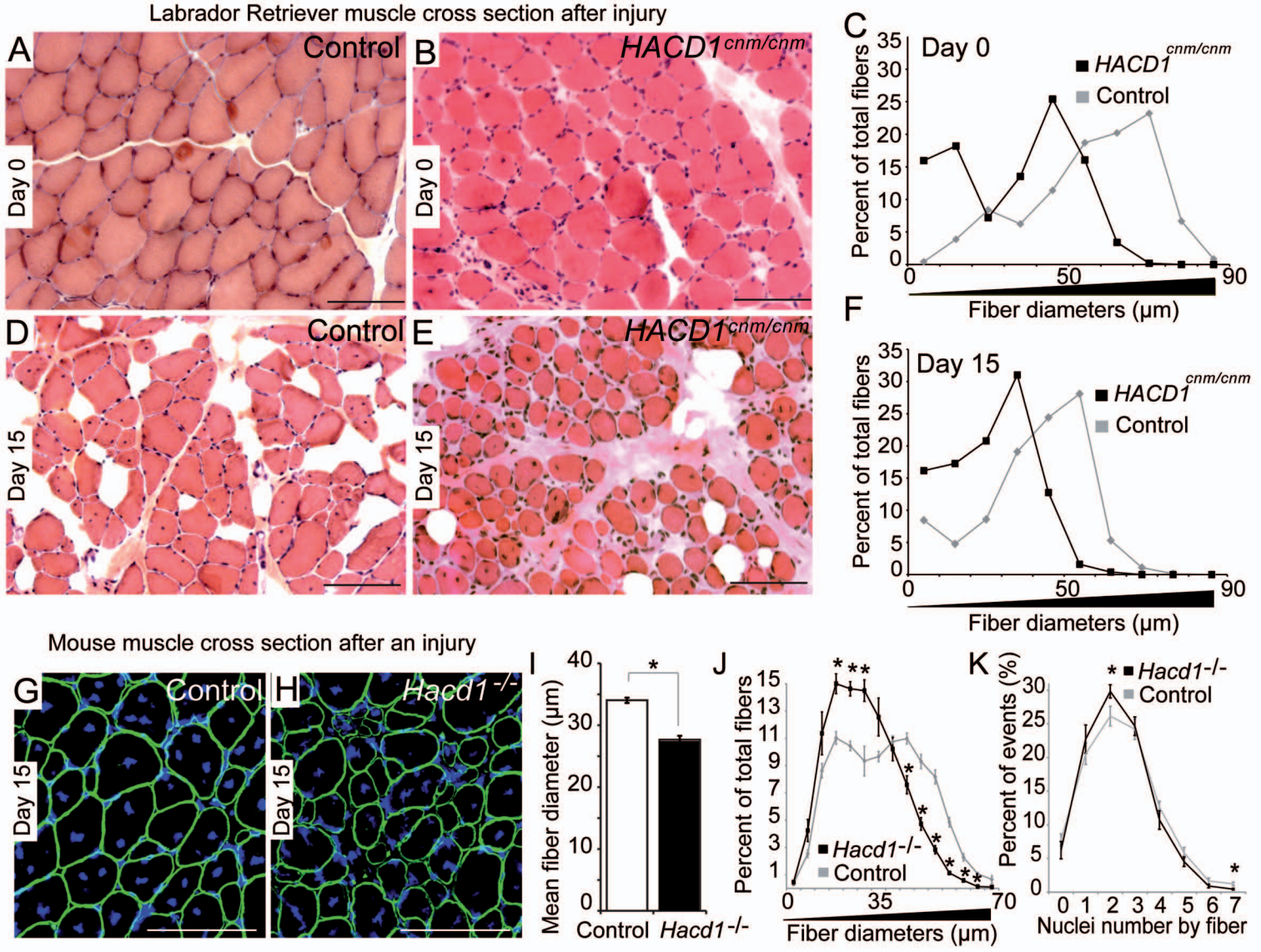
Labrador Retriever muscle cross section after injury
A
Control
Day 0
B
HACD1cnm/cnm
Day 0
C
Day 0
HACD1cnm/cnm
Control
Percent of total fibers
Fiber diameters (μm)
D
Control
Day 15
E
HACD1cnm/cnm
Day 15
F
Day 15
HACD1cnm/cnm
Control
Percent of total fibers
Fiber diameters (μm)
Mouse muscle cross section after an injury
G
Control
Day 15
H
Hacd1-/-
Day 15
I
Mean fiber diameter (μm)
Control
Hacd1-/-
J
Hacd1-/-
Control
Percent of total fibers
Fiber diameters (μm)
K
Hacd1-/-
Control
Percent of events (%)
Nuclei number by fiber

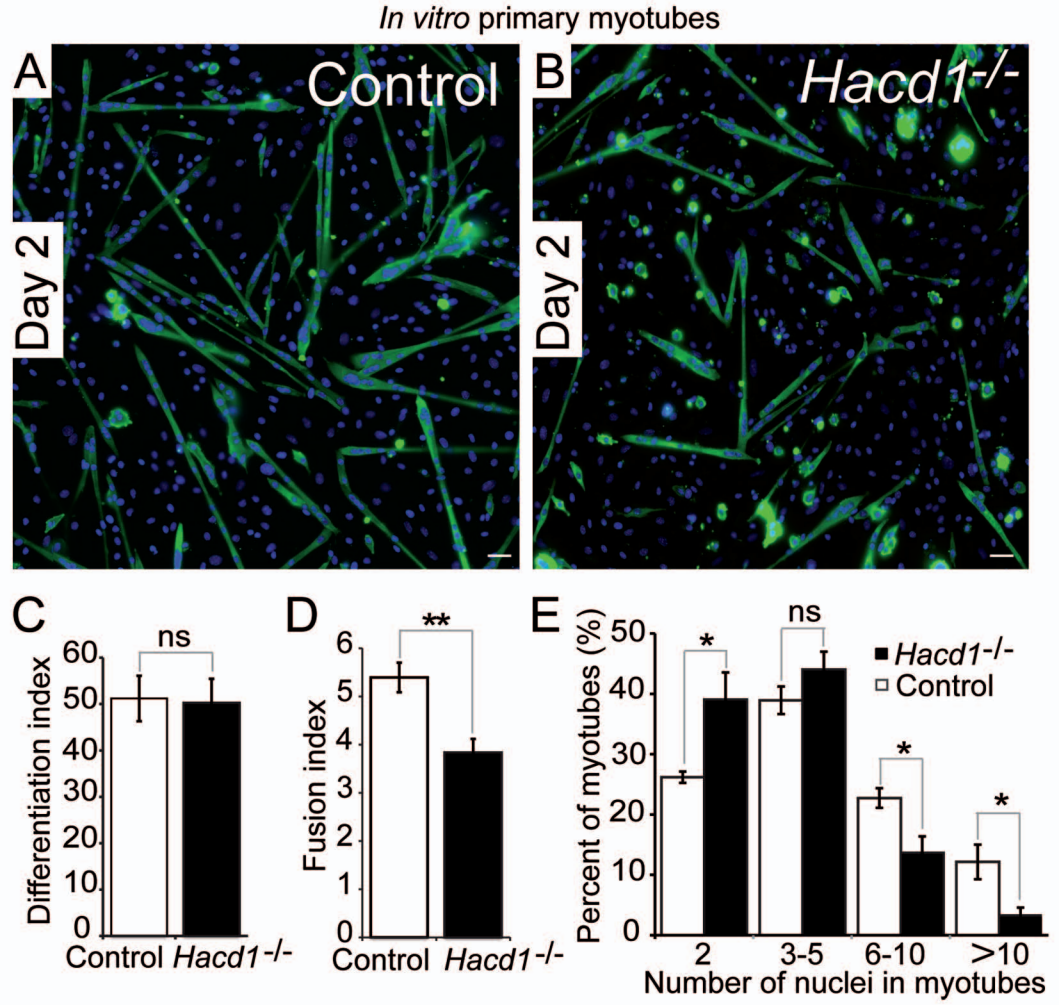
In vitro primary myotubes
A
Control
Day 2
B
Hacd1-/-
Day 2
C
ns
Differentiation index
60
50
40
30
20
10
0
Control
Hacd1-/-
D
**
Fusion index
6
5
4
3
2
1
0
Control
Hacd1-/-
E
*
ns
*
*
Hacd1-/-
Control
Percent of myotubes (%)
50
40
30
20
10
0
2
3-5
6-10
>10
Number of nuclei in myotubes

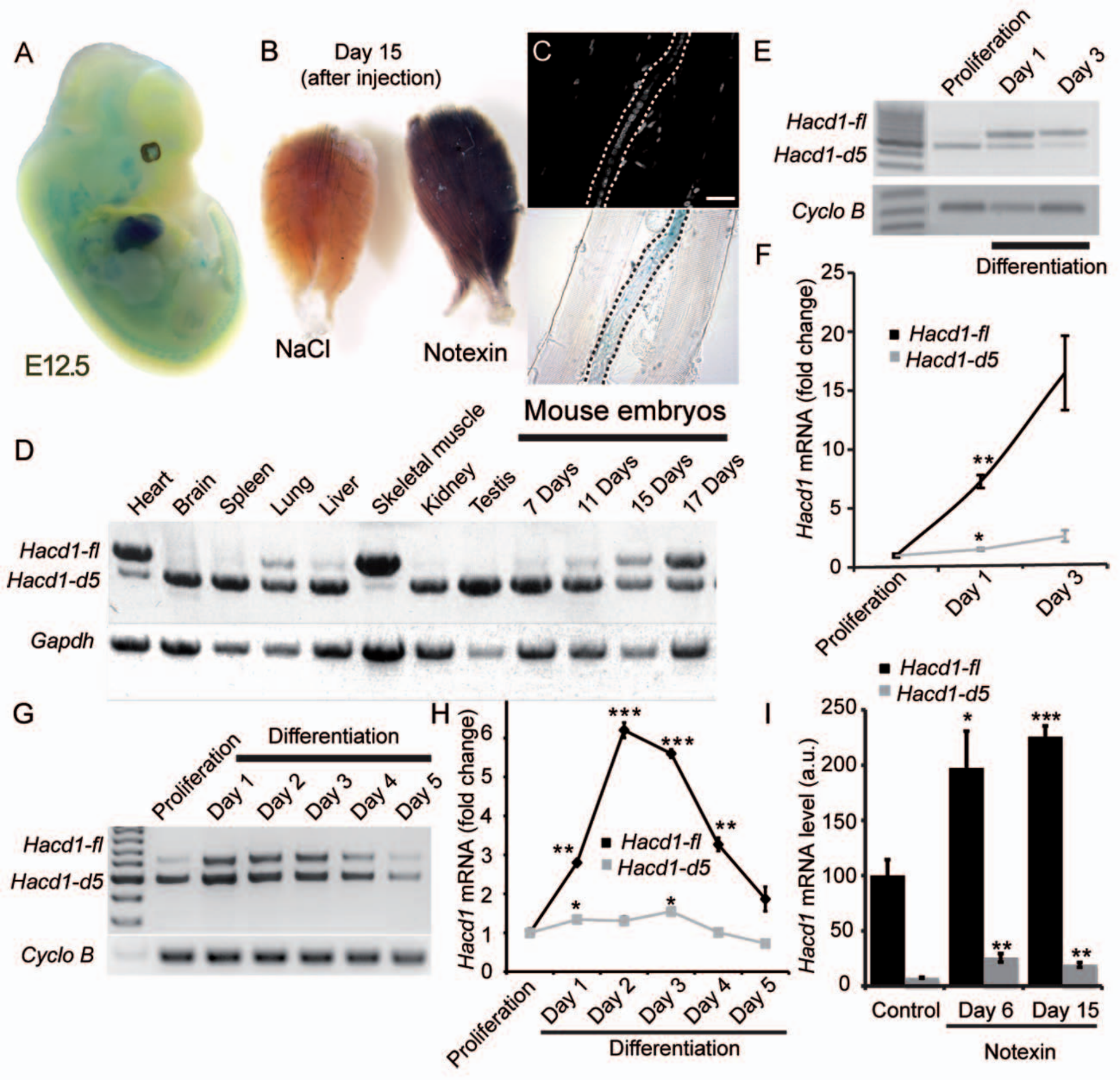
A
E12.5
B
Day 15
(after injection)
NaCl
Notexin
C
E
Proliferation
Day 1
Day 3
Hacd1-fl
Hacd1-d5
Cyclo B
Differentiation
F
Hacd1 mRNA (fold change)
Hacd1-fl
Hacd1-d5
Proliferation
Day 1
Day 3
Mouse embryos
D
Heart
Brain
Spleen
Lung
Liver
Skeletal muscle
Kidney
Testis
7 Days
11 Days
15 Days
17 Days
Hacd1-fl
Hacd1-d5
Gapdh
G
Proliferation
Differentiation
Day 1
Day 2
Day 3
Day 4
Day 5
Hacd1-fl
Hacd1-d5
Cyclo B
H
Hacd1 mRNA (fold change)
Hacd1-fl
Hacd1-d5
Proliferation
Day 1
Day 2
Day 3
Day 4
Day 5
Differentiation
I
Hacd1 mRNA level (a.u.)
Hacd1-fl
Hacd1-d5
Control
Day 6
Day 15
Notexin

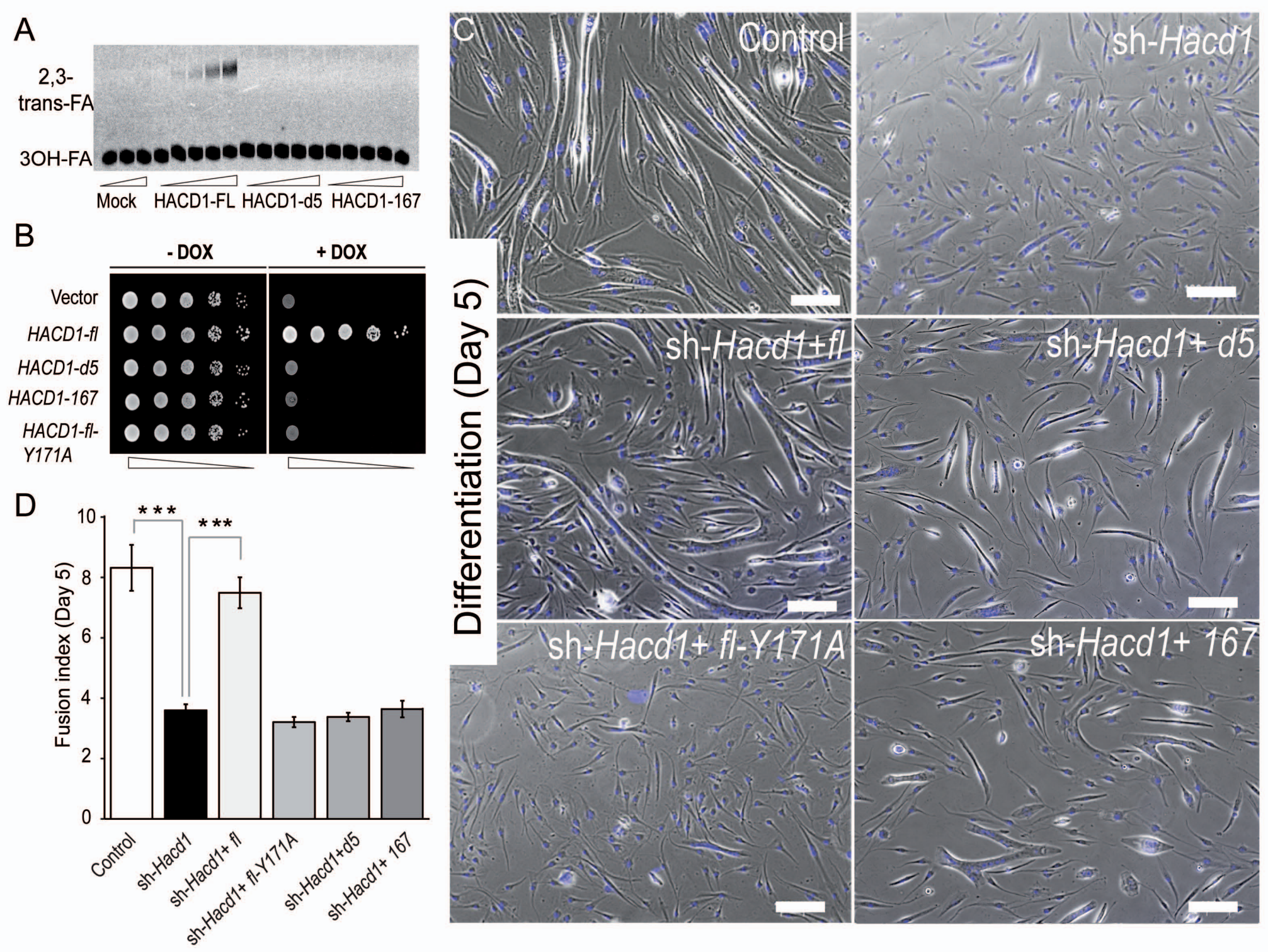
A
2,3-
trans-FA
3OH-FA
Mock
HACD1-FL
HACD1-d5
HACD1-167
B
- DOX
+ DOX
Vector
HACD1-fl
HACD1-d5
HACD1-167
HACD1-fl-
Y171A
C
Control
sh-Hacd1
sh-Hacd1+fl
sh-Hacd1+ d5
sh-Hacd1+ fl-Y171A
sh-Hacd1+ 167
Differentiation (Day 5)
D
Fusion index (Day 5)
10
8
6
4
2
0
***
***
Control
sh-Hacd1
sh-Hacd1+ fl
sh-Hacd1+ fl-Y171A
sh-Hacd1+d5
sh-Hacd1+ 167

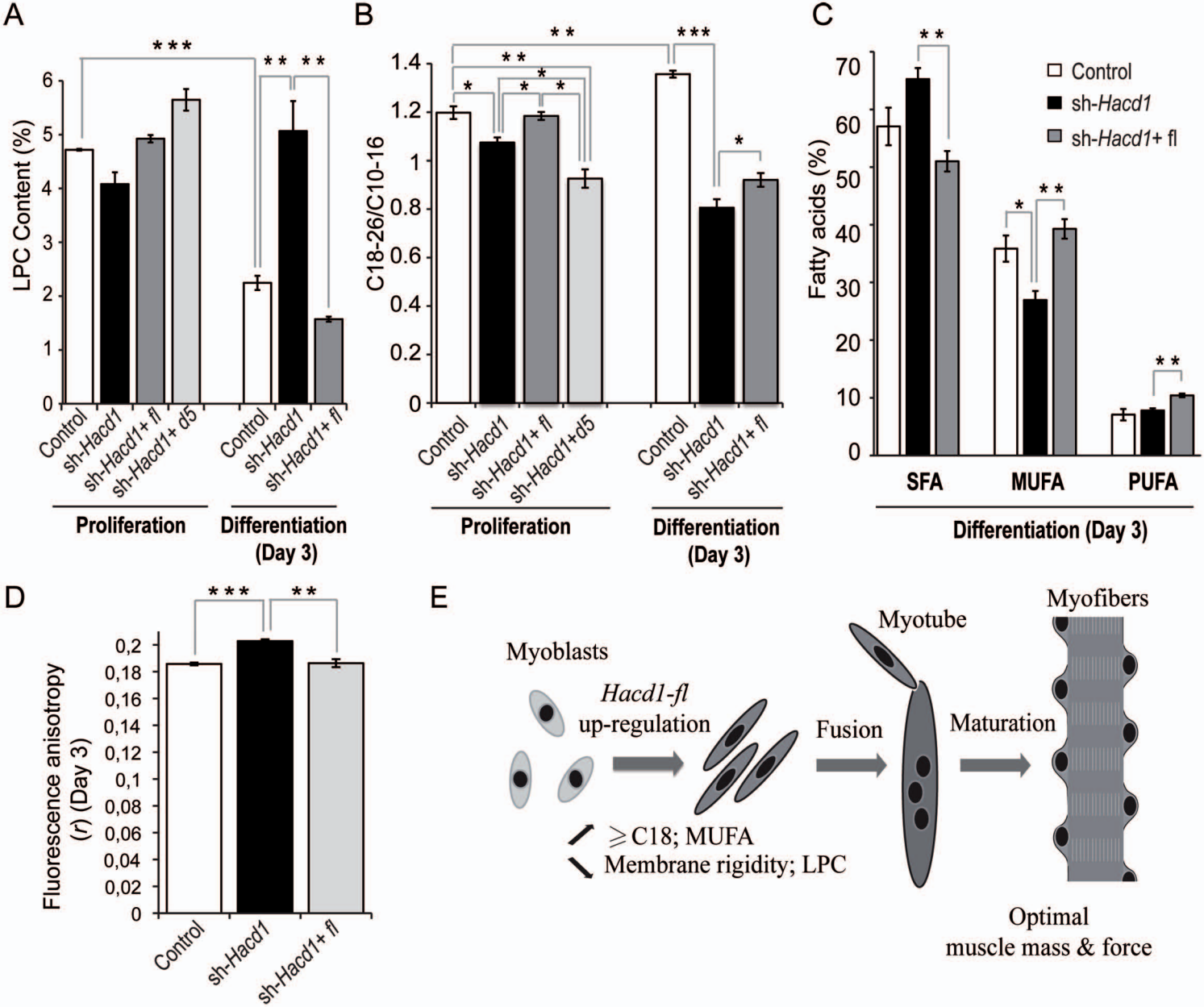
A
LPC Content (%)
Control
sh-Hacd1
sh-Hacd1+ fl
sh-Hacd1+ d5
Proliferation
Differentiation (Day 3)
B
C18-26/C10-16
Control
sh-Hacd1
sh-Hacd1+ fl
sh-Hacd1+d5
Proliferation
Differentiation (Day 3)
C
Fatty acids (%)
Control
sh-Hacd1
sh-Hacd1+ fl
SFA
MUFA
PUFA
Differentiation (Day 3)
D
Fluorescence anisotropy (r) (Day 3)
Control
sh-Hacd1
sh-Hacd1+ fl
E
Myoblasts
Hacd1-fl
up-regulation
Myotube
Fusion
Maturation
Myofibers
⩾C18; MUFA
Membrane rigidity; LPC
Optimal
muscle mass & force

Supplementary material

Animals, Materials and Methods

Generation of *Hacd1* knockout mice

The *Hacd1* knockout recombination vector (PRPGS00067_A_B09) was obtained from the Knockout Mouse Project Repository (KOMP) (https://www.komp.org/). The targeting vector carried *loxP* sites upstream of exon 2 and downstream of exon 4 of *Hacd1* gene and a *NeoR* cassette flanked by two *loxP* sites upstream of exon 2. In order to generate ES cells heterozygous for the targeting vector, the construct was linearized using AsiSI (New England BioLabs), then purified. The vector was electroporated into C57BL/6N ES cells and G418-resistant clones were screened for homologous recombination by PCR (Long Range PCR, dNTPack (Roche)) using the following primers (Forward primer: 5'ATG GGT GCC TAT TTT CAG TCA GTC A-3'; Reverse primer: 5'AAC TGG TTC CTT CAC GAC ATT CAA C-3'). A second PCR was performed to control the presence of *loxP* site upstream of exon 5 (Forward primer: 5'-TCT TAG GAA GGA GAT GGC GCA-3'; Reverse primer: 5'-AGC CAG CAG GGC TAT AAA CTG AGA C-3'). Chromosomal integrity of the selected clones was checked by karyotyping and Southern blotting was performed to confirm the presence of a single insertion.

Positive clones were then injected into BALB/c blastocysts and chimeric males were mated with C57BL/6N females. Presence of the *Hacd1* targeting allele in individuals from the progeny was assessed by PCR (Forward primer: 5'-TTC ATG TGAA CAC ATT TCT ATT C-3'; Reverse primer: 5'-TGT CTT TTT CTC TAA GCT CCT C-3') (PCR was performed as explained below for RT-PCR). Mice carrying the *Hacd1* targeting allele were bred with *PGK-Cre* mice to generate *Cre*-positive mice carrying a recombinant, knockout *Hacd1* allele ($Hacd1^{+/-}$ mice). *PGK-Cre* transgene was eliminated at the following generation and crosses between $Hacd1^{+/-}$ mice generated control (wild type and $Hacd1^{+/-}$) and *Hacd1* knockout ($Hacd1^{-/-}$) mice for the described experiments. All experiments were performed on mice generated from two independent ES clones.

Muscle dissection and regeneration experiment in mice

Male mice were euthanized by cervical dislocation and the *tibialis cranialis* (TA) and *gastrocnemius* muscles were dissected and frozen as described below. For regeneration experiments, 15 µl of Notexin (Latoxan) (10^{-5}M diluted in 0.9% NaCl) were injected into the left TA, and 15 µl of 0.9% NaCl into the right TA (Day 0) of 10 month-old males. Mice were euthanized on Day+6 or Day+15 following notexin injection and TA muscles were dissected and

either frozen for RT-qPCR or immunofluorescence experiments, or stained in X-Gal solution (see below).

X-Gal staining of mouse embryos and muscles

A C57BL6/N mouse female crossed with a *Hacd1*$^{+/-}$ male was euthanized by cervical dislocation at stage E12.5 of gestation. The uterus was dissected in PBS and embryos were extracted and fixed for 1 h in 4% formaldehyde in PBS at 4 °C, then rinsed and stained overnight at 33 °C in a solution of PBS containing 1% Tween 20, 4 mM potassium ferrocyanide, 4 mM potassium ferricyanide, 2 mM MgCl2, 0.4 mg/ml X-Gal dissolved in DMSO (all reagents were from Sigma). Embryos were then rinsed in PBS. No staining was observed in *Hacd1*$^{+/+}$ embryos, other than that typically-occurring very lightly in the intestinal tract. The same protocol was applied to TA muscles at Day+6 following notexin injection.

Maximal muscle force measurement in mice

Tibialis anterior muscles of 6-mo-old males were evaluated by the measurement of in situ isometric muscle contraction in response to nerve stimulation as previously described (Schirwis *et al.*, 2013). Mice were anaesthetised using a pentobarbital solution (ip, 60 mg/kg). Feet were fixed with clamps to a platform and knees were immobilized using stainless steel pins. The distal tendons of muscles were attached to an isometric transducer (Harvard Bioscience) using a silk ligature. The sciatic nerves were proximally crushed and distally stimulated by bipolar silver electrode using supramaximal square wave pulses of 0.1 ms duration. All data provided by the isometric transducer were recorded and analyzed on a microcomputer, using PowerLab system (4SP, AD Instruments). All isometric measurements were made at an initial length L0 (length at which maximal tension was obtained during the tetanus). Responses to tetanic stimulation (pulse frequency from 6.25, 12.5, 25, 50, 100 and 143 Hz) were successively recorded. Absolute maximal tetanic force was determined. Muscle mass (m) was measured to calculate specific maximal force (= absolute maximal force/m). All procedures were performed in accordance with national and European legislations and all experimental protocols have been approved by the French Departmental Direction of Animal Protection (agreement 75-1102).

Muscle biopsy samples and regeneration experiment in dogs

Biceps femoris biopsy samples were collected through an open surgical procedure either once in 5-mo-old or 3- to 5-y-old healthy or *HACD1*$^{cnm/cnm}$ Labrador Retrievers or sequentially before (T0) and 4, 15, 30 and 90 days after the notexin injection in 36- to 48-month-old healthy or CNM

Labrador Retrievers. The venom injection was performed as previously described (Sharp *et al.*, 1993; Wilson *et al.*, 1994).

Ethics statement

The ANSES/EnvA/Upec Ethics Committee (C2EA – 16; www.enseignementsup-recherche.gouv.fr) approved the experiments performed on mice (approval numbers 11/11/15-2 and 20/12/12-16). Labrador Retrievers were dogs maintained in our research colony, and samples used in this study were frozen samples obtained in the 1990s by one of the co-authors (SB). At the time they were sampled, there was no animal welfare committee at the Ecole nationale vétérinaire d'Alfort; however, SB is a certified veterinarian and was accredited by the Veterinary Division of the French Ministry of Agriculture to perform research on animals.

Cell culture

HEK 293T cells were grown in Dulbecco's modified Eagle's medium (DMEM; Sigma, St. Louis, MO), supplemented with 10% fetal bovine serum (FBS) and penicillin/streptomycin, seeded in dishes coated with 0.3% collagen respectively. C2C12 myoblasts were grown in DMEM (PAA) containing 4.5 g/l glucose, supplemented with 15% FBS (PAA) and penicillin/streptomycin. Cells were maintained at 37 °C in a saturated humidity atmosphere containing 5% CO_2. For the differentiation of C2C12 myoblasts, fetal bovine serum was replaced by 2% horse serum (Biowest) when myoblasts reached 70-80% confluence. For fatty acid supplementation, 10 mM fatty acids (Sigma) stock solution maintained at -20 °C in ethanol in glass tubes, were dissolved in DMEM supplemented with 0.25 mM fatty acid-free BSA (Sigma, A6003) at 37 °C for 5 min under strong agitation. Fatty acid solutions were filtrated through 0.2 µm filters (Dutscher, 146560) and diluted in differentiation medium (DMEM + 2% of horse serum) at a final concentration of 5 µM from the first day of differentiation (D0). The fusion index was calculated as the mean number of nuclei per myotube at day 5 of differentiation. Myotubes were defined as myosin heavy chain-positive cells containing at least 2 nuclei.

Primary myoblasts were obtained by dissection of hindlimb muscles from 5-day-old wild type, *Hacd1*$^{+/-}$ and *Hacd1*$^{-/-}$ pups. Muscles were digested in PBS containing 0.5 mg/ml collagenase (GIBCO 17101) and 3.5 mg/ml dispase (GIBCO 17105) for 2 h at 37 °C. Cell suspension was filtered through a 40 µm cell strainer and pre-plated in DMEM + 15% FBS for 4 h at 37 °C, 5% CO_2. Non-adherent myogenic cells were collected and plated in IMDM (GIBCO 31980) + 20% FBS onto Ibidi dishes (Biovalley 80426) coated with collagen (Sigma C7661). Differentiation was triggered by changing the culture media to IMDM + 2% of horse serum for 2 days.

Generation of sh-*Hacd1* cells

Two shRNA pGIPZ lentiviral vectors designed to target *Hacd1* exon 4 (V2LHS_5923 (GCTCATTACTCACAGTATA) and V2LHS_252516 (CTCATTACTCACAGTATAA)) and a control vector (RHS4349; OpenBiosystems) were transfected into C2C12 cells using Arrest-in (OpenBiosystems). After 48h, transfected cells were selected with puromycin (2 mg/ml; Invitrogen). Individual clones were picked after 10 days of selection and shRNA efficiency was checked by RT-qPCR. Initial experiments conducted in parallel in one V2LHS_5923 and one V2LHS_252516 clone proved phenotypic similarity. Clone V2LHS_252516 clone (named sh-*Hacd1* cells) was then selected for the series of functional experiments. Control cells correspond to cells transduced with the control vector.

Transduction of *HACD1* isoforms

For expression of shRNA-resistant isoforms in control and sh-*Hacd1* cells, cDNAs from the three canine *HACD1* isoforms were isolated by RT-PCR on mRNA extracted from muscles of wild type (*HACD1-fl* and *–d5* isoforms) and CNM-affected (*HACD1-167* isoform) Labrador Retrievers. Three silent mutations (GCTCATCACACATAGTATA) were introduced into exon 4 of *HACD1-fl* and *HACD1-d5* cDNAs by PCR and a MYC tag was introduced at the 5' end of the 3 isoforms using the following primers. Forward primer for all isoforms: GATCCTCGAGACCATGGCATCAATGCAGAAGCTGATCTCAGAGGAGGACCTGGCTGCA CTTATGGCGTCCAGCGAGGAG; Reverse primer for *HACD1-fl* and *HACD1-167*: AGATGCGGCCGCTTAATCATCCTTTTCTACAATCACTTCTC; Reverse primer for *HACD1-d5*: AGATGCGGCCGCTCACCAACAACCCCGACAGGA. PCR products were cloned into the pCR4-TOPO vector (Life Technologies). After sequencing, cDNAs were cloned in the MSCV-IRES-BlasticidinR (MSCV-IRES-bsr) retroviral vector using EcoRI restriction. The *HACD1-fl-Y171A* mutation (ATCATCTTAGCTCCTGTCGGGGT) was obtained by PCR from the *HACD1-fl* shRNA-resistant construct and cloned as described.

Retroviral particles were produced by transient triple transfection of HEK293T cells with XtremeGene 9 reagent from Roche, according to manufacturer's instructions, using a 2:1:1 ratio of MSCV-ires-bsr, LTR-env and CMV-gag-pol (a kind gift of Olivier Albagli). Retroviral supernatants were collected 48 h after transfection and concentrated on Amicon Ultra-15 centrifugal

filter units (100 kDa cut-off, Millipore). C2C12 cells were spinfected by a 1 h centrifugation (300 g) in the presence of retroviral supernatant and 8 µg/ml polybrene (Sigma).

Tranduced cells were selected with blasticidin (5 µg/ml; Invitrogen). Plasmid expression was checked by RT-qPCR and immunostaining.

Extraction of total RNA, RT-PCR and RT-qPCR analysis

Mouse muscle samples were snap frozen in liquid nitrogen and stored at -80 °C. Total RNAs were isolated from C2C12 myoblasts and mouse samples with RNA Nucleospin Kit (Macherey-Nagel) according to the manufacturer's protocol. Purity of RNAs was assessed by a ratio of absorbance at 260 nm and 230 nm > 1.7. RNA quality was checked on agarose gel. One microgram of RNA was used for reverse transcription with the Maxima First Strand cDNA Synthesis Kit for RT-qPCR (Fermentas). cDNA were amplified using the Maxima SYBR Green qPCR Master Mix (2X) (Fermentas). PCR reactions were performed with Taq DNA Polymerase from MP Biomedicals on a Mastercycle Eppendorf thermocycler. qPCR reactions were performed on a Roche Light Cycler Carousel-based system 2.0 (Roche).

Expression of mouse *Hacd1* and *glyceraldehyde 3-phosphate dehydrogenase* (*Gapdh*) mRNAs were examined by PCR using first-strand cDNAs from various mouse tissues and embryonic stages (Mouse MTC panel I; Clontech, TAKARA Bio, Palo Alto, CA, USA) with primer pairs (for *Hacd1*, Hacd1-For-2/Hacd1-Rev-2; and *Gapdh*, Gapdh-For/Gapdh-Rev). These and the other primers used for quantification of gene expression are listed in Table S1. All PCR and qPCR products were examined qualitatively on agarose gels. All presented RT-qPCR results were normalized to *Tbp1* (*Hacd1* expression during muscle regeneration), *Hprt1* (*Pax7* expression) or *CycloB* (all other cases) gene expression.

Immunofluorescence and histological staining

Control, sh-*Hacd1* or sh-*Hacd1* cells expressing shRNA-insensitive isoforms were grown for 48 h on a glass coverslip (Menzel-Glaser) and then briefly rinsed three times with PBS (PAA), fixed for 15 min with 4% formaldehyde and rinsed with PBS. Cells were permeabilized for 10 min with PBS-0.1% Triton (Sigma), rinsed 3 times with PBS, and blocked with PBS-1% BSA (Sigma) for 1 h before incubation with antibodies. Primary anti-Calnexin (rabbit polyclonal, Sigma, 1:200), anti-Myc (mouse 4A6, Millipore, 1:200), and anti-myosin heavy chain (mouse MF20, DSHB, 1:500) antibodies were incubated overnight at 4 °C and revealed using secondary Alexa 488 goat anti-rabbit (1:500) and Alexa 555 goat anti-mouse (1:500) (Invitrogen). Nuclei were stained with DAPI (4',6' diamidino-2-phenylindol) 1:4000 for 10 min at RT and slides were mounted using

Fluorescent mounting medium (Dako). Alternatively, they were mounted in aqueous mountant containing the chromatin stain DAPI (1.5 µg/ml) (Vectorshield).

Muscle biopsy samples from dogs and muscles from mice were snap-frozen in isopentane cooled in liquid nitrogen and stored at −80 °C. Transverse-sections (10 µm thickness) were stained with hematoxylin-eosin (H&E) or in an ATPase staining solution following a preincubation at pH = 9.4 or immunostained as previously described for cells with anti-Pax7 (mouse monoclonal, DSHB, 1:20), anti-V5 epitope (rabbit polyclonal, Abcam, 1:500, anti-Ryr1 (mouse Abcam 3C, 1:100) primary antibodies. For Dystrophin immunostaining, fixation was performed with acetone/methanol v/v at -20 °C for 15 min and immunostaining was pursued with anti-Dystrophin (mouse monoclonal, Novocastra, 1:20) antibody. For both anti-PAX7 and anti-Dystrophin antibodies, Mouse Ig Blocking Reagent (MOM kit, Vector, MFB-2213) was used following the manufacturer's instructions. Alexa 488 or 594 goat anti-rabbit (1:500) and Alexa 488 or 555 goat anti-mouse (1:500) (Invitrogen) secondary antibodies were then used. Images were captured using an Axio Observer Z1 microscope (Zeiss) and analyzed using Photoshop CS3.

Routine muscle histopathological evaluation was conducted on the basis of the H&E staining. Diameter and distribution of myofiber type were examined on ATPase 9.4 sections. Quantification of fiber number, size or nuclear content was performed on 7 randomly-selected fields (dog samples) or 3 sections separated by at least 30 µm (mouse samples). Morphometric quantification of the minimal Feret's diameter was done using the Visilog software (Noesis) and quantification of fiber number and nuclear content was done using ImageJ (1.47v). In dog and mouse samples, 500 to 1000 fibers and 700 to 1500 fibers, respectively, were analyzed for each section.

Plasmid electroporation into murine skeletal muscle

V5-tagged murine *Hacd1-fl* was generated by direct TOPO TA cloning of RT-PCR products into pcDNA3.1/V5-His TOPO (Invitrogen) (primer sequences Forward: 5'-GTCACCATGGCGTCCAGTGAGGAG-3' Reverse: 5'-GTGTGTGGGAACCACTAAAT-3'). Expression vector was electroporated into *tibialis cranialis* (TA) muscles of 7-wk-old female C57BL/6 mice (2 mice bilaterally) according to (McMahon *et al.*, 2001). Mice were anaesthetised with fentanyl/fluanisone (Hypnorm) and midazolam (Hynovel) and injected intramuscularly with bovine testes hyaluronidase (25 µl/muscle of 0.4 µg/µl solution in sterile saline) using an insulin syringe and 28 gauge needle. After 2 h, anaesthesia was deepened with isofluorane inhalation, and 25 µl plasmid solution (0.5 µg/µl) was injected into the TA prior to transcutaneous electroporation performed by applying a potential difference of 81V across the muscle in 10 x 20 ms pulses at 1 Hz frequency (ElectroSquare Porator ECM 830, BTX). After 6 days, mice were euthanized by cervical

dislocation and the TA muscles were dissected and treated as described in the previous section.

Yeast strain and media

S. cerevisiae strain TH_3237 (*MAT**a** his3*D*1 leu2*D*0 met15*D*0 ura3*D*0 URA3::CMV-tTA pPHS1::KanMX4-TetO$_7$-CYC$_{TATA}$*) (Mnaimneh *et al.*, 2004) was obtained from Open Biosystems (Huntsville, AL). Cells were grown in synthetic complete (SC) medium (0.67% yeast nitrogen base, 2% D-glucose, and nutritional supplements) but lacking histidine (SC-His) at 30 ˚C.

Western blot analysis

sh-*Hacd1* cells expressing shRNA-insensitive isoforms were washed in PBS and put in lysis buffer (50 mM HEPES pH 7.4, 150 mM NaCl, 0.5% Triton X-100, 10% glycerol, 1 mM DTT, Complete protease inhibitor cocktail (Roche), 1 mM EDTA) for 30 min on ice. Lysates were sonicated and spun for 10 min at 10,000 g. After determination of protein contents using the Bradford method, 20 µg of clarified lysates were separated by SDS-PAGE. Transfer was done on a PVDF membrane (Millipore). Membranes were blocked with TBS-5% skimmed milk for 1 h at RT and incubated with anti-MYC antibody (Mouse 9E10, Sigma, 1:2000) or mouse anti-α-Tubulin (mouse DM1A, Sigma, 1:5000) in TBS-0.1% Tween overnight at 4 °C. After washing, anti-mouse-HRP antibody (Amersham) was applied for 1 h at RT. After washing, antibody-bound proteins were visualised using the ECL+ kit (Amersham). Acquisition was done using a Fusion Fx5 (Vilber Lourmat). Quantification was performed using Photoshop CS3.

Western blot analysis for yeast proteins was performed as described previously (Kihara and Igarashi, 2002), using the anti-FLAG antibody M2 (1 mg/ml; Stratagene, Agilent Technologies, La Jolla, CA, USA) and anti-Pgk1 antibodies (0.25 mg/ml; Molecular Probes, Life Technologies, Eugene, OR) as the primary antibodies, and HRP-conjugated anti-mouse IgG F(ab')$_2$ fragments (at 1:7500 dilution; GE Healthcare Life Sciences, Buckinghamshire, UK) as the secondary antibodies. Labeling was detected using Pierce Western Blotting Substrate (Thermo Fisher Scientific, Waltham, MA, USA).

Co-Affinity Purification (Co-AP) experiments in HEK293T

cDNAs for *cHACD1-fl, -d5* and *-167* isoforms were cloned as baits in the pDEST27-GST Gateway vector (Invitrogen). cDNAs for *cHACD1-fl, -d5* and *-167* isoforms, and human *HACD2*, *HACD3*, *HACD4*, *ELOVL1* to *7*, *KAR* and *TER* genes were cloned as preys in the pCE-puro 3XFlag-1 vector. Human *EIF2B1* cDNA was cloned in the pDEST-Myc Gateway vector (gift from Marc Vidal's lab) as a control prey. For each interaction assay, GST-bait and Flag/Myc-prey expression vectors were co-transfected in HEK293T cells using calcium phosphate. Each Flag/Myc-prey vector was also co-

transfected with GST vector alone. After 24 h, cells were harvested and lysed with lysis buffer (50 mM HEPES pH = 7.4, 150 mM NaCl, 0.5% Triton X-100, 10% glycerol, 1 mM DTT, 1 mM EDTA, Complete protease inhibitor cocktail (Roche)) for 20 min on ice. Cell lysates were sonicated and pre-cleared by centrifugation for 10 min at 15,000 g at 4 °C. Pre-cleared lysates were incubated with Immobilized Glutathione beads (Perbio) for 1 h at 4 °C. Beads were then washed extensively three times with lysis buffer and then eluted with ½ lysis buffer and ½ loading buffer 2X (125 mM Tris pH = 7.4, 4% SDS, 20% glycerol, bromophenol blue) at 37 °C for 5 min. After denaturation, 15 μg of pre-cleared lysates and a constant volume of eluates were separated by SDS-PAGE and transferred to a PVDF membrane (Millipore). FLAG-, MYC- and GST-tagged proteins were detected as described above, using mouse anti-FLAG (M2, 1:2000), mouse anti-MYC (9E10, 1:2000) and rabbit anti-GST (1:2000) antibodies (Sigma), respectively. FLAG-/MYC-tagged proteins were first revealed, membranes were then stripped using Restore Western Blot Stripping Solution (Pierce) and GST-tagged proteins were revealed with ECL+ reagent (Amersham). Acquisition was done using Fusion Fx5 (Vilber Lourmat).

HACD activity assay

The assay was performed using 3-hydroxy[1-^{14}C]palmitoyl-CoA (55 mCi/mmol; American Radiolabeled Chemicals, St. Louis, MO, USA) as described previously (Kihara *et al.*, 2008).

Lipids analyses

Cell preparation

C2C12 cells were rinsed using 0.9% NaCl, trypsinated and resuspended with proliferation medium. Cells were centrifuged at 4,000 g for 10 min and pellets were rinsed twice using 0.9% NaCl. Tubes containing dry pellets were filled with non-reactive argon to prevent aerial oxidation of samples and then immediately frozen at -80 °C.

Reagents

LCMSMS quality grade solvents were purchased from Fischer Scientific (Illkirch, France). Heptadecanoïc acid, tricosanoic acid, pentafluorobenzyl bromide, N,N'-diisopropylethylamine, potassium hydroxide and BHT were purchased from Sigma Aldrich (Saint-Quentin Fallavier, France). Di-myristoyl phosphatidylcholine (DMPC), 19:0-lysophosphatidylcholine (19:0-LPC), di-myristoyl phosphatidylethanolamine (DPME), di-myristoyl phosphatidylserine (DMPS), d18:1-17:0 sphingomyelin (17:0-SM) were from Avanti Polar Lipids (Coger, Paris, France).

Quantitation of total fatty acids by GC-MS

Tissues (ca. 10 mg) were saponified with 1 ml of ethanolic potassium hydroxide (final concentration 0.6 N) containing heptadecanoic acid (10 µg), tricosanoic acid (250 ng) used as internal standards (IS) and 50 mg/l of BHT. Samples were incubated at 56 °C for 45 min under argon. Saponified fatty acids were extracted with 1 ml of HCl 1.2 M and 2 ml of hexane. After evaporation of the organic upper phase under vacuum fatty acids were derivatized to pentafluorobenzyl esters with 5 µl of pentafluorobenzyl bromide, 5 µl of diisopropylbenzylamine and 100 µl of acetonitrile at room temperature for 30 min. Derivatized fatty acids were further extracted with 1 ml of water and 2 ml of hexane. The organic phase was evaporated under vacuum. Finally fatty acids were dissolved in 100 µl prior to GC-MS quantification.

Fatty acids esters (1 µl) were injected in split mode on a HP7890A Gas Chromatograph equipped with an HP7683 injector and a HP5975C Mass Selective Detector (Agilent Technologies). Chromatography was performed using a HP-5MS fused silica capillary column (30 mm x 0.25 mm inner diameter, 0.25 m film thickness, Agilent Technologies). The GC-MS conditions were as follows: carrier gas, helium at a flow-rate of 1.1 ml/min; injector temperature, 250 °C, split mode; oven temperature 140 °C, increased at 5 °C/min to 300 °C, and held for 10 min. The mass spectrometer was operated under negative chemical ionization mode with methane as reactant gaz. The ion source temperature and the quadrupole temperature were 150 °C and 106 °C, respectively.

Quantitation of fatty acids was performed by calculating their relative response ratios to heptadecanoic acid and tricosanoic acid (IS). For this purpose molecular ion responses obtained in negative SIM mode were used.

Quantitation of PC, SM, PS, PE, PI by LCMS-MS

Cells were spicked with DMPC (1.323 nmol), 19:0-LPC (1.380 nmol), DMPE (1.398 nmol), DMPS (1.083 nmol), 17:0-SM (1.194 nmol) used as internal standards and total lipids were further extracted according to the method of Folch *et al*. (Folch *et al.*, 1957).

Analysis of phospholipids was conducted by LCMS-MS in MRM mode as previously described (Vial *et al.*, 2014).

Membrane fluidity assay

Plasma membrane fluidity was estimated by fluorescence anisotropy (*r*) as described (Bastiaanse *et al.*, 1995; Le Borgne *et al.*, 2012). (*r*) measurements were conducted using 1,6 diphenyl 1,3,5 hexatriene (DPH) as a probe. In polarized excitation light, a high *r* value reflects increased rotational lifetime of DPH that happens when DPH orientation is stabilized in less fluid membranes. Cultured cells were rinsed, harvested and centrifuged at 1,000 g for 5 min at 4 °C. The resulting

pellets were resuspended in Opti-MEM® Reduced Serum Medium (Life Technologies, Saint Aubin, France) at a concentration of one million cells per ml. Two milliliters of cell suspension were placed into a 1 cm path length spectroscopic quartz cuvette (VWR International, Limonest, France). The cells were stirred and maintained in a thermostatically controlled chamber. After 6 min at 37 °C, 2 µl of the fluorescent probe DPH (1 mM in tetrahydrofuran) were added to label plasma membranes. *r* was measured at 37 °C 10 min after addition of the probe; after this first series of measurement, the temperature of the chamber was gradually reduced and anisotropy was measured at 35, 30, 25, 20, 15, 10 and 5 °C. Data were expressed as mean ± s.e.m. of three to five independent experiments.

Statistical analysis

ANOVA with repeated measure factor was applied to paired data, i.e. in the case of measurement of fiber number, size, nuclear content or PAX7-positive cell content on muscle sections, as well as mass measurements of paired muscles in mice. Student T test was used for all other analyses and Welch modification was applied when sample number was low ($n < 4$). Data are expressed as mean ± standard error of the mean and differences were considered statistically significant when $P < 0.05$.

Supplementary material references

Bastiaanse EML, Atsma DE, Vandervalk LJM, Vanderlaarse A. Metabolic Inhibition of Cardiomyocytes Causes an Increase in Sarcolemmal Fluidity Which May Be Due to Loss of Cellular Cholesterol. Arch. Biochem. Biophys. 1995; 319: 350–354.

Le Borgne F, Guyot S, Logerot M, Beney L, Gervais P, Demarquoy J. Exploration of Lipid Metabolism in Relation with Plasma Membrane Properties of Duchenne Muscular Dystrophy Cells: Influence of L-Carnitine [Internet]. PLoS ONE 2012; 7[cited 2014 Aug 2] Available from: http://www.ncbi.nlm.nih.gov/pmc/articles/PMC3507830/

Folch J, Lees M, Sloane Stanley GH. A simple method for the isolation and purification of total lipides from animal tissues. J. Biol. Chem. 1957; 226: 497–509.

Kihara A, Igarashi Y. Identification and characterization of a Saccharomyces cerevisiae gene, RSB1, involved in sphingoid long-chain base release. J. Biol. Chem. 2002; 277: 30048–30054.

Kihara A, Sakuraba H, Ikeda M, Denpoh A, Igarashi Y. Membrane topology and essential amino acid residues of Phs1, a 3-hydroxyacyl-CoA dehydratase involved in very long-chain fatty acid elongation. J. Biol. Chem. 2008; 283: 11199–11209.

McMahon JM, Signori E, Wells KE, Fazio VM, Wells DJ. Optimisation of electrotransfer of plasmid into skeletal muscle by pretreatment with hyaluronidase -- increased expression with reduced muscle damage. Gene Ther. 2001; 8: 1264–1270.

Mnaimneh S, Davierwala AP, Haynes J, Moffat J, Peng W-T, Zhang W, et al. Exploration of essential gene functions via titratable promoter alleles. Cell 2004; 118: 31–44.

Schirwis E, Agbulut O, Vadrot N, Mouisel E, Hourdé C, Bonnieu A, et al. The beneficial effect of myostatin deficiency on maximal muscle force and power is attenuated with age. Exp. Gerontol. 2013; 48: 183–190.

Sharp NJ, Kornegay JN, Bartlett RJ, Hung WY, Dykstra MJ. Notexin-induced muscle injury in the dog. J. Neurol. Sci. 1993; 116: 73–81.

Vial G, Chauvin M-A, Bendridi N, Durand A, Meugnier E, Madec A-M, et al. Imeglimin Normalizes Glucose Tolerance and Insulin Sensitivity and Improves Mitochondrial Function in Liver of a High-Fat High-Sucrose Diet Mice Model. Diabetes 2014

Wilson LA, Cooper BJ, Dux L, Dubowitz V, Sewry CA. Expression of utrophin (dystrophin-related protein) during regeneration and maturation of skeletal muscle in canine X-linked muscular dystrophy. Neuropathol. Appl. Neurobiol. 1994; 20: 359–367.

Legends to Supplementary Figures

Supplementary Fig. 1. Generation and analysis of *Hacd1* knockout mice. (**A**) Representation of the *Hacd1* locus, the structure of the targeting vector, and the organization of the rearranged *Hacd1* knockout allele after CRE-mediated recombination. (**B**) PCR genotyping of wild type, $Hacd1^{+/-}$ and $Hacd1^{-/-}$ mice. (**C**) RT-qPCR experiments for expression of *Hacd1* isoforms and *Hacd2* and *Hacd3* genes in TA muscles from wild type and $Hacd1^{-/-}$ mice (n = 3 for each condition). Note that expression of *Hacd2* and *Hacd3* genes was not modified in *Hacd1*-KO mice. *Hacd4* expression was not observed in either condition (data not shown). (**D**) Tibial length in wild type or $Hacd1^{+/-}$ (control) and $Hacd1^{-/-}$ 6 mo-old mice (n = 9 and 4 mice, respectively). (**E**) Mean specific maximal force (*i.e.,* the ratio of absolute force to muscle mass) of TA muscles from $Hacd1^{-/-}$, $Hacd1^{+/-}$ and wild type mice (n = 8, 6 and 8, respectively). (**F**) Photographs of a control and a $Hacd1^{-/-}$ 12-mo-old mouse. Note the kyphosis (red arrow) in the $Hacd1^{-/-}$ mouse. (**G**) H&E-stained transverse-sections of TA muscles at Day 6 after notexin injection in control and $Hacd1^{-/-}$ mice. Bars: 100 µm. Error bars correspond to standard error of the mean. *: $P < 0.05$; **: $P < 0.01$; ***: $P < 0.001$.

Supplementary Fig. 2. Weight gain and regeneration experiment in $HACD1^{cnm/cnm}$ dogs. (**A**) Total weight of $HACD1^{+/cnm}$ (control) and $HACD1^{cnm/cnm}$ pups of a same litter from birth to 28 days (n = 3 for each group). (**B**) Total weight of $HACD1^{+/cnm}$ (control) and $HACD1^{cnm/cnm}$ 2-mo-old pups (n = 7 and 13, respectively). Error bars correspond to standard error of the mean. *: $P < 0.05$. (**C**) H&E-staining on muscle sections before (Day 0) and at Day 4, 15, 30 or 90 after notexin injection in $HACD1^{+/cnm}$ (control) and $HACD1^{cnm/cnm}$ muscles (n=1 for each condition). Bars: 200 µm.

Supplementary Fig. 3. Progenitors in mice and expression of *Hacd* genes in myoblasts. (**A** and **B**) Immunofluorescence for PAX7 (in red) and Dystrophin (in green) on TA muscle cross-sections in control (**A**) and $Hacd1^{-/-}$ (**B**) mice. Nuclei are stained in blue. Asterisks point to PAX7-positive nuclei. (**C**) TA muscle area per PAX7-positive, satellite cells as observed in (**A** and **B**) (n = 3 mice per condition; more than 70 PAX7-positive cells examined per mouse). (**D**) RT-qPCR experiments for *Pax7* expression in TA muscles from control and $Hacd1^{-/-}$ mice (n = 4 for each condition). Error bars correspond to standard error of the mean. (**E**) Expression of *Hacd1* isoforms and *Hacd2* and *Hacd3* genes during C2C12 differentiation. Results of RT-qPCR experiments are expressed as a percentage of the level of the *Hacd1-fl* isoform at Day 2 (n = 3 for each condition). Error bars correspond to standard error of the mean. *: $P < 0.05$; **: $P < 0.01$; ***: $P < 0.001$.

Supplementary Fig. 4. Conformation, expression, HACD activity and interactions of HACD1 isoforms. (**A**) Topological structure of HACD1 isoforms predicted by the SOSUI program. Blue and pink residues are important and essential residues for HACD activity, respectively. Y171 residue (red square) was replaced by an A residue in HACD1-FL-Y171A construct. (**B**) Expression of Myc-tagged HACD1 isoforms in the ER of C2C12 myoblasts decorated with an anti-Calnexin antibody. Nuclei are stained in blue. (**C**) In mouse muscle section, a V5-tagged HACD1-FL isoform also localizes at the sarcoplasmic reticulum decorated with an anti-RyR1 antibody. Bars: 10 μm. (**D**) Co-Affinity Precipitation (Co-AP) experiments between HACD1 isoforms and other members of the Very Long Chain Fatty Acid elongation complex. GST-tagged HACD1 isoforms or the empty GST vector (baits) were co-expressed in HEK293T cells with 3xFLAG-tagged protein members of the complex, or with the MYC-tagged EIF2B1 taken as a negative control (preys). Eluates were revealed for GST (upper panel) and FLAG/MYC (mid panel). Expression of FLAG/MYC-tagged proteins was checked in total lysates (lower panel). Data are representative of two to three independent experiments. (**E**) Quantity of the 2,3-trans hexadecenoic acid produced by each HACD1 isoform (Fig. 6A) and expressed as a percentage of the initial quantity of substrate. Error bars correspond to standard error of the mean. (**F**) Quantities of 3xFLAG-tagged HACD1 isoforms in total yeast lysates (Fig. 6B) checked by western blotting (upper panel) and normalized to Pgk1 (lower panel).

Supplementary Fig. 5. Characterization of sh-*Hacd1* cells. (**A**) Expression of each *Hacd1* isoform by RT-qPCR in sh-*Hacd1* cells compared to control cells, both in proliferation and at Day 3 of differentiation. Data are expressed as a percentage of expression in control cells (n = 3 for each condition). Error bars correspond to standard error of the mean. *: $P < 0.05$; **: $P < 0.01$; ***: $P < 0.001$. (**B-C**) RT-qPCR experiments for *Myogenin* (**B**) and *Myosin, heavy polypeptide 2, skeletal muscle, adult (Myh2)* (**C**) gene expression in control and sh-*Hacd1* cells during differentiation. Significant differences in expression between proliferation and during differentiation are shown for each condition. (**D**) Immunofluorescence in sh-*Hacd1* cells at Day 5 of differentiation. Myosin heavy chains (MHC) are stained in green, actin in red and nuclei in blue. (**E**) Expression of Myc-tagged HACD1 isoforms in the ER of sh-*Hacd1* myoblasts decorated with an anti-Calnexin antibody. Nuclei are stained in blue; bars: 10 μm. (**F**) Total cell lysates from sh-*Hacd1* and isoform-expressing sh-*Hacd1* cells were subjected to immunoblotting using antibodies raised against Myc (upper panel) and Tubulin as a control of loading (lower panel).

Supplementary Fig. 6. Unsaturation level of phospholipid fatty acid and membrane fluidity in sh *Hacd1* cells. (**A**) Proportions of saturated (SFA), monounsaturated (MUFA) or polyunsaturated

(PUFA) fatty acids in proliferation (n = 3 for each condition; error bars correspond to standard error of the mean). (**B**) Fluorescence anisotropy (*r*, inverse of fluidity) measured at Day 3 of differentiation from 5°C to 37°C. For each cell type, the measured anisotropy increased when the temperature decreased, demonstrating that the DPH probe was in a lipid environment (n = 3 for each condition). Error bars correspond to standard error of the mean. *: $P < 0.05$; ***: $P < 0.001$.

Supplementary Table 1

Primer name *	Sequence
cHacd1-ex1F	5’-CCTTCTACATCGCCATGACC-3’
cHacd1-ex7R	5’-CACCTTGTTCAGGGGGATCATT-3’
cHacd1-fl-For	5’-TATGGTGTGGCTCATCACACAT-3’
cHacd1-fl-Rev	5’-TGGCCCATTTAATGAAGTATGGC-3’
cHacd1-d5-For	5’-TATGGTGTGGCTCATCACACAT-3’
cHacd1-d5-Rev	5’-CAATGGTATATATGAGGCCATGG-3’
cHacd1-167-For	5’-TCGCCATGACCTCGGGATAC-3’
cHacd1-167-Rev	5’-CAATGGTATATATGAGGCCATGG-3’
Hacd1-ex1F	5'-GCCTGGCTCACCTTCTACAAT-3'
Hacd1-ex7R	5'-CGTGGAGCACCTTTCTTCTC-3'
Hacd1-For	5’-ATATCCCGTTGGAGTTGCTG-3’
Hacd1-Rev	5’-CGTGGAGCACCTTTCTTCTC-3’
Hacd1-fl-For	5’-ATGAAGAGAGCGTGGTGCTT-3’
Hacd1-fl-Rev	5’-AAGGCGGCGTATATTGTGAG-3’
Hacd1-For-2	5’-ATGGCGTCCAGTGAGGAGGACGGC-3’
Hacd1-Rev-2	5’-TTAATCGTCCTTCTCCGCGATC-3’
Hacd1-d5-For	5’-TCACAGTATAAAACCCATACAATT-3’
Hacd1-d5-Rev	5’-GAGGCCATGGTTATGAGAAG-3’
Hacd1-167-For	5’-AATATCGCCATGACGGCCGGATAC-3’
Hacd1-167-Rev	5’-CAACGGTATATAGGAGGCCATG-3’
cycloB-For (*Ppib* gene)	5’-GATGGCACAGGAGGAAAGAG-3’
cycloB-Rev (*Ppib* gene)	5’-AACTTTGCCGAAAACCACAT-3’
Hacd2-For	5’-TGCTATAGGGATTGTGCCATC-3’
Hacd2-rev	5’-ACGGATAATTTCCGTGATTGTCC-3’
Hacd3-For	5’-GACGTGCAGAACCCTGCTATC-3’
Hacd3-Rev	5’-CTTCTGGACTGTGATGTTCACC-3’
Hacd4-For	5’-CAGCTCACAGAGAGAGTGATC-3’
Hacd4-Rev	5’-GAGTGTTTGACTGAGCCATGTC-3’
Myogenin-For	5’-CTACAGGCCTTGCTCAGCTC-3’
Myogenin-Rev	5’-AGATTGTGGGCGTCTGTAG-3’
Myh2-For	5’-ACTGGAGGGTGAGGTAGAGAG-3’
Myh2-Rev	5’-GCCTCCTCAGCTTGTCTCTTG-3’
Gapdh-For	5’-TGAAGGTCGGTGTCAACGGATTTGGC-3’
Gapdh-Rev	5’-CATGTAGGCCATGAGGTCCACCAC-3’
Pax7-For	5’-AGGCCTTCGAGAGGACCCAC-3’
Pax7-Rev	5’-CTGAACCAGACCTGGACGCG-3’
TBP-For	5’-ATCCCAAGCGATTTGCTG-3’
TBP-Rev	5’-CCTGTGCACACCATTTTTCC-3’
Hprt1-For	5'-GTTAAGCAGTACAGCCCCAAA-3'
Hprt1-Rev	5'-AGGGCATATCCAACAACAAACTT-3'

*c: canine sequence; otherwise: mouse sequence

Supplementary Table 2

A

		Proliferation			Differentiation (Day 3)		
Phospholipids (%)	Control (a)	*sh-Hacd1* (b)	*sh-Hacd1+fl* (c)	*sh-Hacd1+d5* (d)	Control (e)	*sh-Hacd1* (f)	*sh-Hacd1+fl* (g)
PC	55.067±0.213^{b,d,f,g}	53.263±0.219^{a,d,f,g}	53.650±0.411^{d,f,g}	46.935±0.076^{g}	48.368±2.175	47.328±1.214^{a,b,c}	50.391±0.064^{a,b,c,d}
PI	20.129±0.381^{c,d,e,g}	17.967±0.942^{e,g}	14.512±1.403^{a,e,f,g}	15.484±0.988^{a,e,f,g}	30.913±2.386^{a,b,c,d}	22.315±1.736^{c,d}	24.834±0.156^{a,b,c,d}
PE	9.108±0.368^{b,c,d,g}	11.905±0.328^{a,e}	12.322±0.551^{a,e}	12.048±0.251^{a,e}	8.510±0.365^{b,c,d,g}	11.334±1.040	11.499±0.180^{a,e}
PS	3.202±0.046^{g}	3.060±0.026^{g}	2.823±0.159^{g}	2.920±0.177^{g}	3.244±0.100^{g}	3.557±0.343	3.840±0.103^{a,b,c,d,e}
SM	5.619±0.144^{b,c,d,f,g}	7.671±0.179^{a,d,e,f}	9.304±0.928^{a,d,e}	14.500±0.960^{a,b,c,e,f,g}	5.416±0.114^{b,c,d,f,g}	9.111±0.217^{a,b,d,e,g}	7.093±0.024^{a,d,e,f}
LPC	4.718±0.016^{e,g}	4.080±0.221^{d,e,g}	4.924±0.069^{e,g}	5.648±0.201^{b,e,g}	2.246±0.132^{a,b,c,d,f,g}	5.066±0.559^{e,g}	1.572±0.047^{a,b,c,d,e,f}
LPE	2.156±0.145^{e,f,g}	2.053±0.141^{e,f,g}	2.464±0.019^{e,f,g}	2.463±0.232^{e,f,g}	1.304±0.046^{a,b,c,d,g}	1.289±0.086^{a,b,c,d,g}	0.772±0.011^{a,b,c,d,e,f}

B

		Proliferation			Differentiation (Day 3)		
LPC (% of phospholipids)	Control (a)	*sh-Hacd1* (b)	*sh-Hacd1+fl* (c)	*sh-Hacd1+d5* (d)	Control (e)	*sh-Hacd1* (f)	*sh-Hacd1+fl* (g)
14:0	0.104±0.001^{c,g}	0.092±0.005^{c,d,g}	0.115±0.003^{a,b,e,g}	0.169±0.017^{b,e,g}	0.088±0.004^{c,d,g}	0.562±0.116	0.071±0.003^{a,b,c,d,e}
16:0	1.799±0.007^{d,e,g}	1.610±0.098^{d,e,g}	1.937±0.051^{d,e,g}	2.174±0.028^{a,b,c,e,g}	0.953±0.058^{a,b,c,d,f,g}	2.518±0.279^{e,g}	0.648±0.020^{a,b,c,d,e,f}
18:0	0.518±0.003^{e,f,g}	0.439±0.025^{d,e,f,g}	0.513±0.008^{e,f,g}	0.663±0.061^{b,e,g}	0.313±0.018^{a,b,c,d,f,g}	1.275±0.178^{a,b,c,e,g}	0.236±0.011^{a,b,c,d,e,f}
18:1	2.064±0.022^{b,e,f,g}	1.722±0.083^{a,c,e,f,g}	2.099±0.039^{b,e,f,g}	2.068±0.139^{e,f,g}	0.770±0.004^{a,b,c,d,g}	0.588±0.087^{a,b,c,d}	0.491±0.012^{a,b,c,d,e}
18:2	0.149±0.019	0.150±0.006^{d,e,g}	0.153±0.017	0.218±0.000^{b,e,g}	0.099±0.009^{b,d}	0.197±0.031	0.109±0.003^{a,b,c,d,e}
20:4	0.082±0.003^{d,e,f,g}	0.094±0.003^{d,e,g}	0.102±0.007^{d,e,g}	0.250±0.003^{a,b,c,e,f,g}	0.009±0.013^{a,b,c,d,f}	0.111±0.005^{a,d,e,g}	0.014±0.001^{a,b,c,d,e,f}

Legend. Repartition of (**A**) phospholipid species and (**B**) LPC species in control, *sh-Hacd1* and isoform expressing sh-*Hacd1* cells in proliferation and at Day 3 of differentiation. The amount of each species is expressed as its mole fraction to the total content (mol %; n = 3 for each condition). Superscript letters indicate significant differences ($P < 0.05$) with values reported in columns named using a one-letter-code. For example, the value of LPC in differentiating control cells ($2.246\pm0.132^{a,b,c,d,f,g}$) is significantly different from all the other values [(a,b,c,d,f,g) columns], and LPC in differentiating *sh-Hacd1* is significantly different from values of LPC in control and *sh-Hacd1+fl* cells [(e,g) columns].

Supplementary Table 3

A

	Proliferation				Differentiation (Day 3)		
Fatty acids (%)	Control (a)	*sh-Hacd1* (b)	*sh-Hacd1+fl* (c)	*sh-Hacd1+d5* (d)	Control (e)	*sh-Hacd1* (f)	*sh-Hacd1+fl* (g)
10:0	0.170±0.029^{e}	0.170±0.04	0.087±0.009^{d}	0.249±0.045^{c}	0.069±0.011^{a,g}	0.438±0.142	0.334±0.039^{e}
12:0	0.357±0.042^{c,d}	0.412±0.051^{c,d}	0.163±0.003^{a,b,d}	0.607±0.02^{a,b,c}	0.251±0.067^{f,g}	1.149±0.184^{e}	0.694±0.106^{e}
14:0	3.371±0.294^{e}	3.338±0.134^{c}	2.914±0.072^{b}	3.216±0.153	6.308±0.172^{a,f,g}	4.977±0.263^{e}	4.741±0.182^{e}
16:0	34.701±1.509^{c,d,e}	37.257±0.339^{c,d}	27.492±0.497^{a,b,d}	42.282±0.821^{a,b,c}	23.939±1.009^{a,f,g}	40.131±0.072^{e,g}	33.915±0.904^{e,f}
18:0	16.185±0.295^{b,c,e}	14.765±0.287^{a,c}	11.695±0.598^{a,b,d}	16.063±0.801^{c}	26.232±2.050^{a,f,g}	18.031±0.234^{e,g}	11.028±0.642^{e,f}
20:0	0.066±0.004^{b,d,e}	0.085±0.004^{a,c}	0.066±0.002^{b,d}	0.114±0.012^{a,c}	0.209±0.013^{a,g}	0.224±0.009^{g}	0.120±0.020^{e,f}
22:0	0.030±0.001^{b,c,d,e}	0.042±0.001^{a,c}	0.035±0.000^{a,b,d}	0.060±0.007^{a,c}	0.025±0.001^{a,f,g}	0.104±0.009^{e,g}	0.058±0.010^{e,f}
24:0	0.040±0.002^{b,c,d,e}	0.070±0.003^{a,d}	0.075±0.001^{a}	0.115±0.015^{a,b}	0.010±0.001^{a,f,g}	0.159±0.015^{e,g}	0.094±0.015^{e,f}
26:0	0.009±0.002^{b,d,e}	0.017±0.001^{a,c}	0.009±0.000^{b,d}	0.028±0.005^{a,c}	0.001±0.000^{a,g}	0.037±0.019	0.026±0.004^{e}
16:1 n-7	4.136±0.748^{c,d,e}	3.891±0.146^{c,d}	10.196±0.298^{a,b,d}	2.201±0.087^{a,b,c}	8.574±0.583^{a,f}	3.882±0.167^{e,g}	7.063±0.595^{f}
16:1 n-9	2.769±0.2^{c}	3.135±0.097^{c}	3.919±0.122^{a,b,d}	2.892±0.266^{c}	3.283±0.441	4.836±0.538	4.775±0.325
18:1 n-7	4.650±0.374^{c,d,e}	4.137±0.214^{c,d}	8.099±0.256^{a,b,d}	2.921±0.141^{a,b,c}	7.684±0.582^{a,f,g}	2.255±0.102^{e,g}	4.637±0.464^{e,f}
18:1 n-9	19.364±1.097^{c,d}	19.636±0.469^{c,d}	26.164±0.308^{a,b,d}	15.196±0.439^{a,b,c}	16.06±0.641^{g}	15.131±0.769^{g}	22.226±1.081^{e,f}
20:1	0.180±0.016^{b,c,d}	0.309±0.037^{a}	0.238±0.020	0.344±0.039^{a}	0.186±0.027^{f}	0.710±0.106^{e}	0.481±0.109
22:1	0.035±0.001^{b,d,e}	0.055±0.004^{a,c}	0.039±0.002^{b,d}	0.065±0.007^{a,c}	0.065±0.008^{a,f}	0.118±0.016^{e}	0.084±0.022
24:1	0.011±0.001^{b,c,d}	0.019±0.001^{a,c,d}	0.022±0.001^{a,b,d}	0.031±0.002^{a,b,c}	0.016±0.002	0.021±0.001	0.020±0.003
18:2	1.22±0.05^{b,d,e}	1.435±0.007^{a,c}	1.358±0.016^{b}	1.469±0.056^{a}	2.427±0.266^{a,f,g}	3.400±0.193^{e}	3.879±0.193^{e}
18:3	0.143±0.021	0.133±0.001^{d}	0.140±0.003^{d}	0.100±0.004^{b,c}	0.156±0.023^{f,g}	0.283±0.020^{e,g}	1.028±0.123^{e,f}
20:3	2.367±0.086^{c,d,e}	2.225±0.057^{c}	2.759±0.091^{a,b,d}	1.997±0.081^{a,b,c}	0.653±0.081^{a,f,g}	1.251±0.053^{e,g}	2.142±0.142^{e,f}
20:4	4.6±0.479^{c,e}	4.087±0.074^{c,d}	2.119±0.060^{a,b,d}	5.370±0.177^{b,c}	1.677±0.287^{a}	1.152±0.048	1.185±0.073
20:5	0.442±0.01^{c,d,e}	0.438±0.006^{c,d}	0.372±0.013^{a,b,d}	0.497±0.012^{a,b,c}	0.997±0.191^{a}	0.715±0.034	1.059±0.068
22:4	0.533±0.087^{c,e}	0.454±0.006^{c,d}	0.143±0.002^{a,b,d}	0.540±0.002^{b,c}	0.082±0.013^{a}	0.114±0.006	0.088±0.010
22:5	2.491±0.243^{c,e}	2.060±0.024^{c,d}	0.959±0.008^{a,b,d}	2.167±0.015^{b,c}	0.578±0.109^{a}	0.530±0.025	0.532±0.041
22:6	2.104±0.092^{b,c,d,e}	1.800±0.039^{a,c,d}	0.925±0.033^{a,b,d}	1.441±0.051^{a,b,c}	0.484±0.082^{a}	0.344±0.013^{g}	0.500±0.048^{f}
24:4	ND	ND	ND	ND	0.007±0.000	ND	ND
24:5	ND	ND	ND	ND	0.005±0.001	ND	ND
24:6	0.026±0.003^{c,e}	0.029±0.001^{c,d}	0.014±0.000^{a,b,d}	0.025±0.000^{b,c}	0.008±0.001^{a}	0.006±0.000	0.007±0.001

B

	Proliferation				Differentiation (Day 3)		
Fatty acids (%)	Control (a)	*sh-Hacd1* (b)	*sh-Hacd1+fl* (c)	*sh-Hacd1+d5* (d)	Control (e)	*sh-Hacd1* (f)	*sh-Hacd1+fl* (g)
C18-C26/C10-C16	1.198±0.026^{b,d,e,f,g}	1.074±0.021^{a,c,d,e,f,g}	1.185±0.016^{b,d,e,f,g}	0.926±0.037^{a,b,c,e,f}	1.357±0.014^{a,b,c,d,f,g}	0.805±0.035^{a,b,c,d,e,g}	0.921±0.028^{a,b,c,e,f}

C

	Proliferation				Differentiation (Day 3)		
Fatty acids (%)	Control (a)	*sh-Hacd1* (b)	*sh-Hacd1+fl* (c)	*sh-Hacd1+d5* (d)	Control (e)	*sh-Hacd1* (f)	*sh-Hacd1+fl* (g)
SFA	54.928±1.670^{c,d,f}	56.157±0.815^{c,d,f}	42.536±0.685^{a,b,d,e,f,g}	62.734±0.878^{a,b,c,g}	57.048±3.265^{c}	65.252±1.935^{a,b,c,g}	51.010±1.774^{c,d,f}
MUFA	31.146±2.387^{c,d}	31.181±0.662^{c,d,g}	48.677±0.511^{a,b,d,e,f,g}	23.651±0.581^{a,b,c,e,g}	35.872±2.283^{c,d,f}	26.953±1.563^{c,e,g}	39.286±1.699^{b,c,d,f}
PUFA	13.926±0.757^{c,e,f,g}	12.662±0.175^{c,e,f,g}	8.788±0.220^{a,b,d,g}	13.615±0.350^{c,e,f,g}	7.080±0.991^{a,b,d}	7.795±0.379^{a,b,d,g}	10.420±0.318^{a,b,c,d,f}

Legend. Phospholipid fatty acid sorted by their content (**A**), length ratio (**B**) and saturation classes (**C**) of control, *sh-Hacd1* and isoform expressing sh-*Hacd1* cells in proliferation and at Day 3 of differentiation. Total phospholipid fatty acid methyl esters are presented depending of their aliphatic chain and saturation degree. The amount of each fatty acid is expressed as its mole fraction to the total free fatty acid content (mol %; n = 3 for each condition). Superscript letters indicate significant differences ($P < 0.05$) with values reported in columns named using the one-letter-code described in Supplementary Table 2.

Supplementary Figure 1

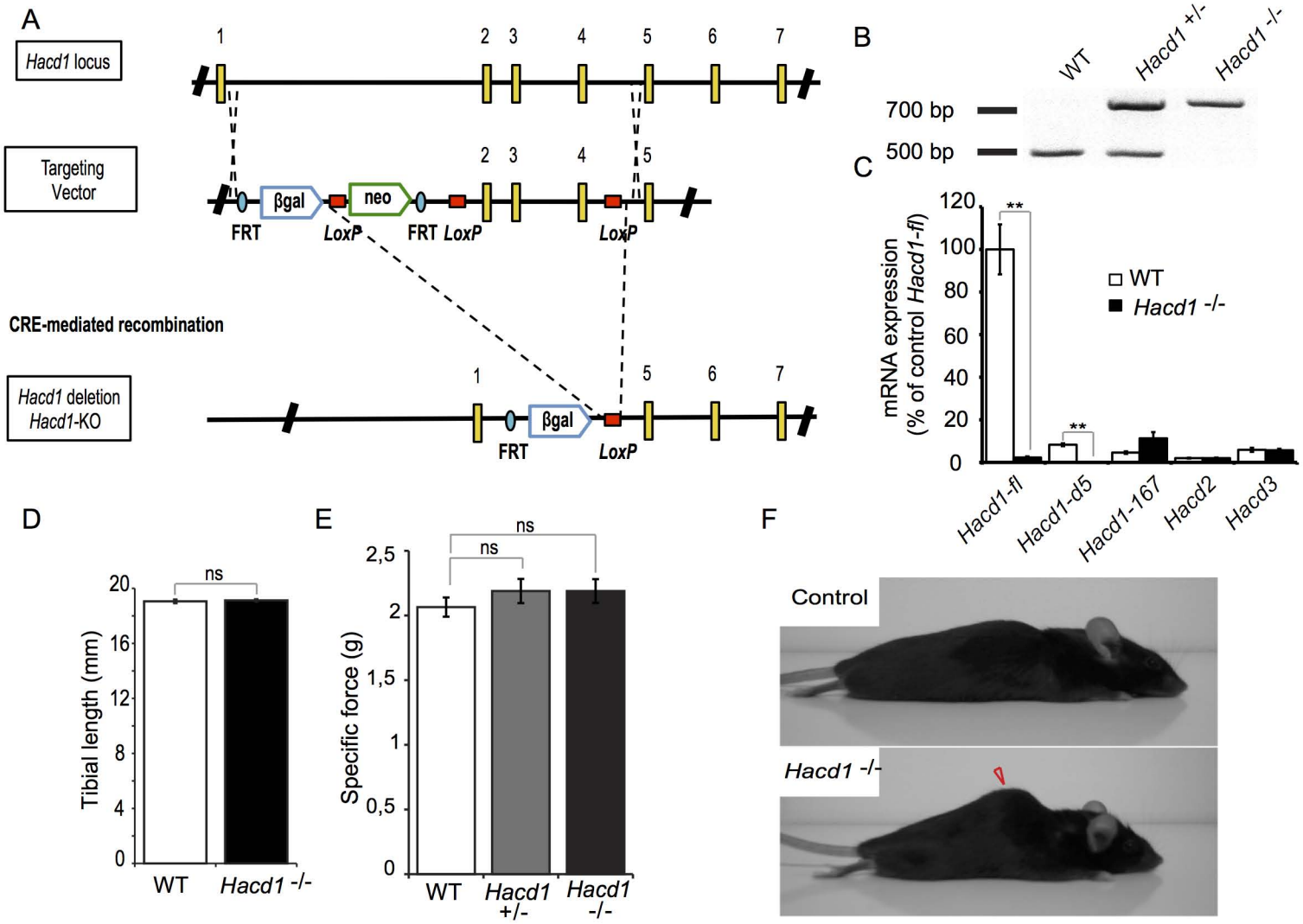

G

At day 6 after notexin injection

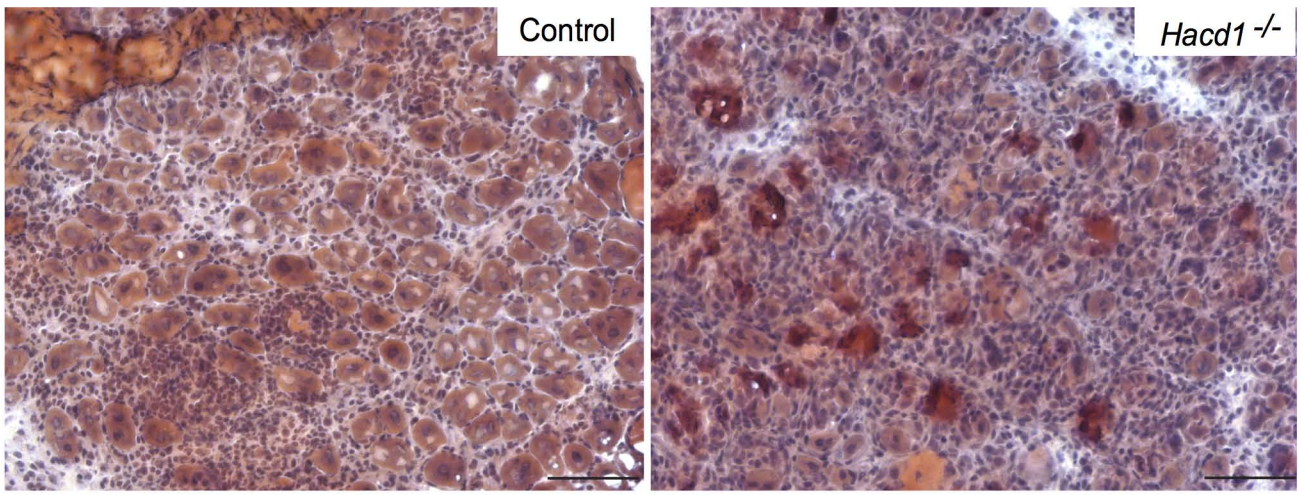

Supplementary Figure 2

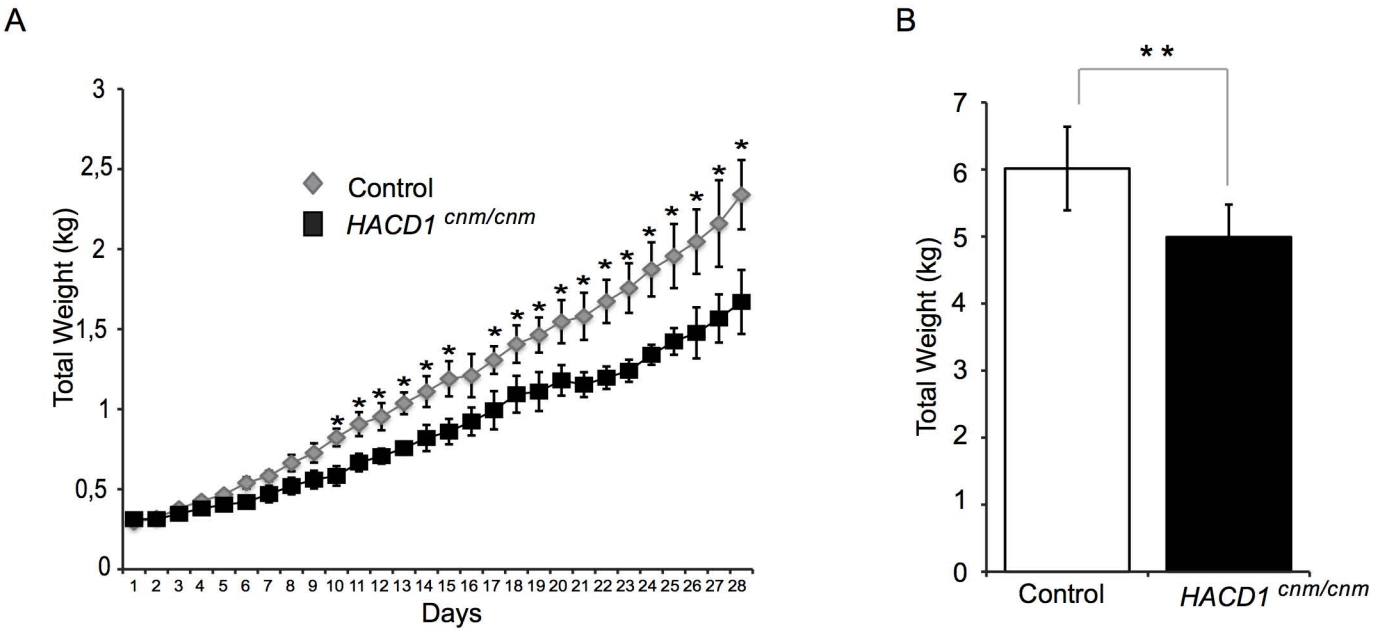

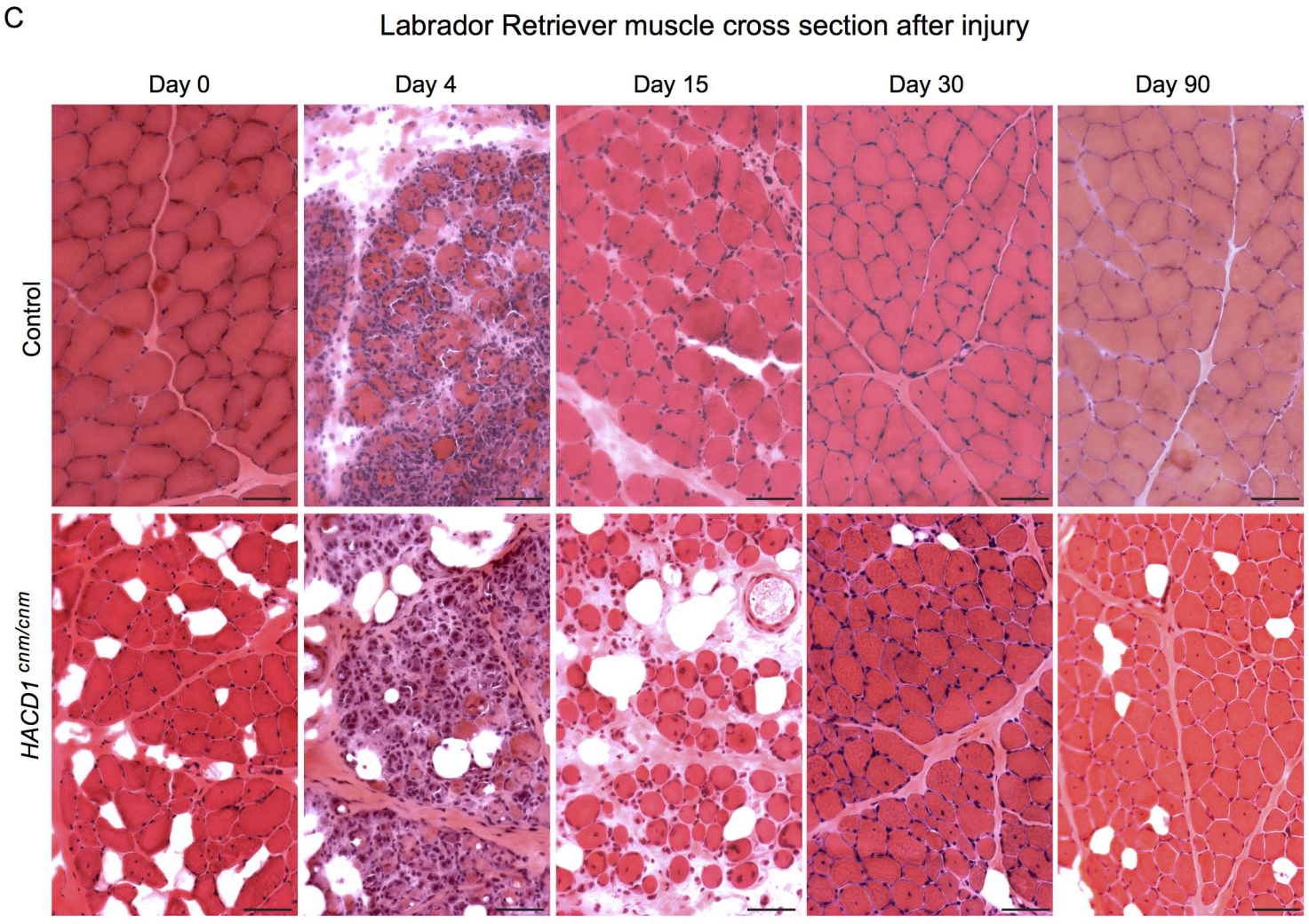

Supplementary Figure 3

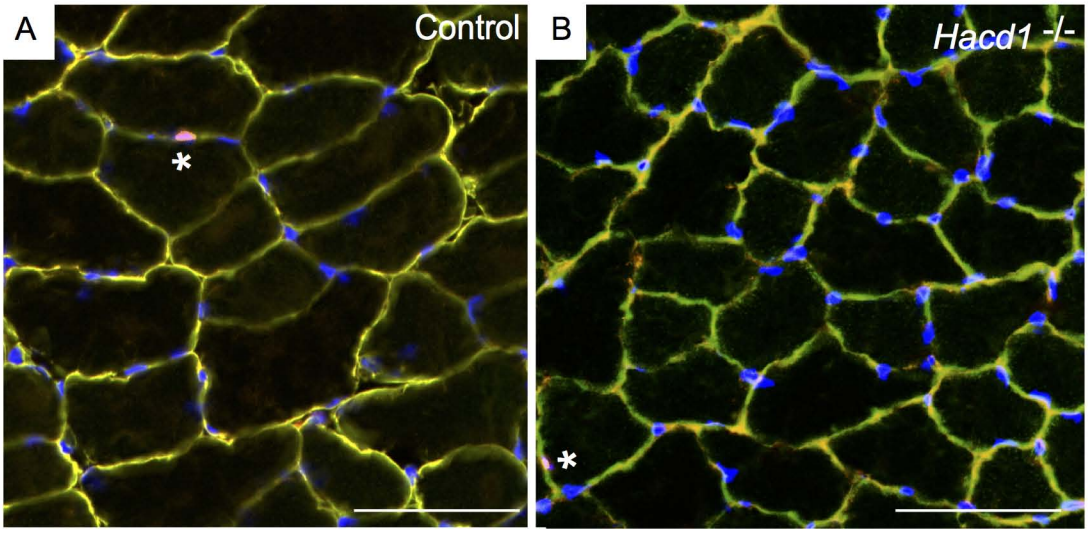

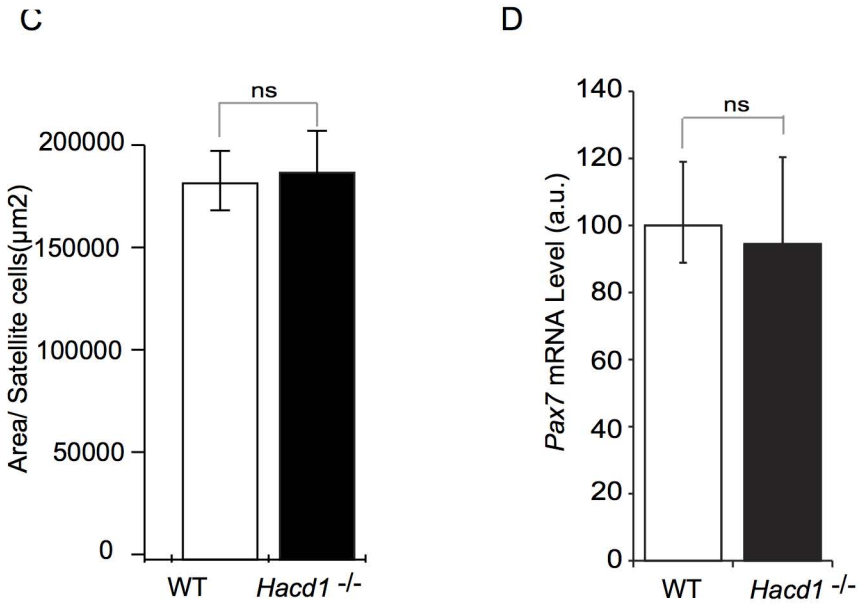

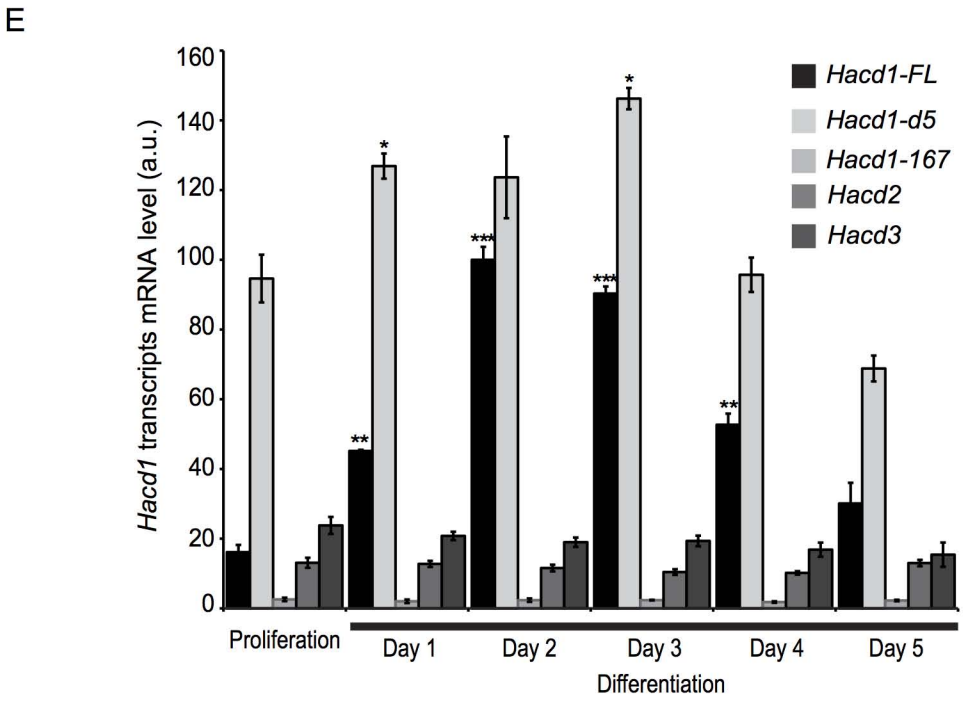

Supplementary Figure 4

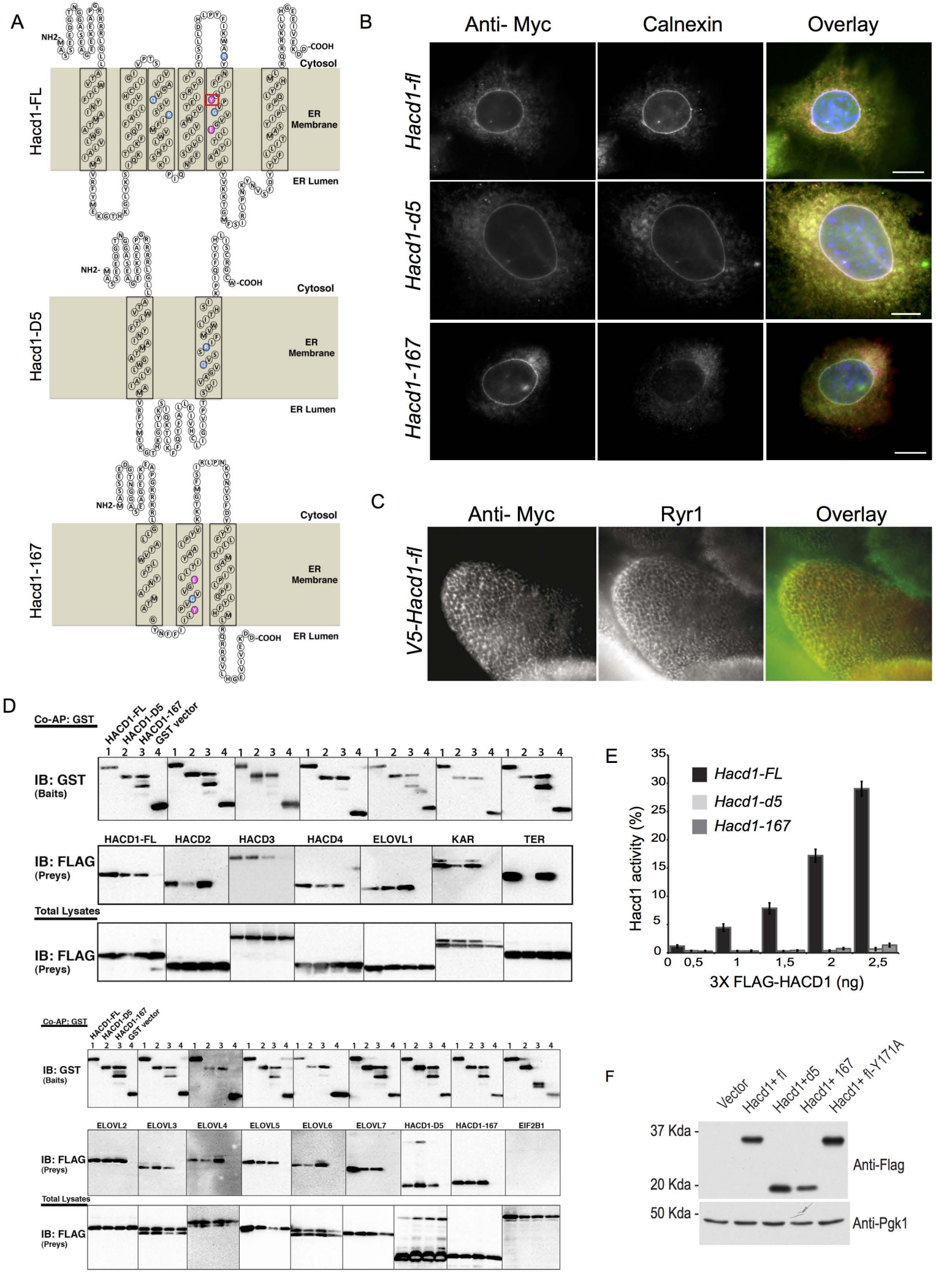

Supplementary Figure 5

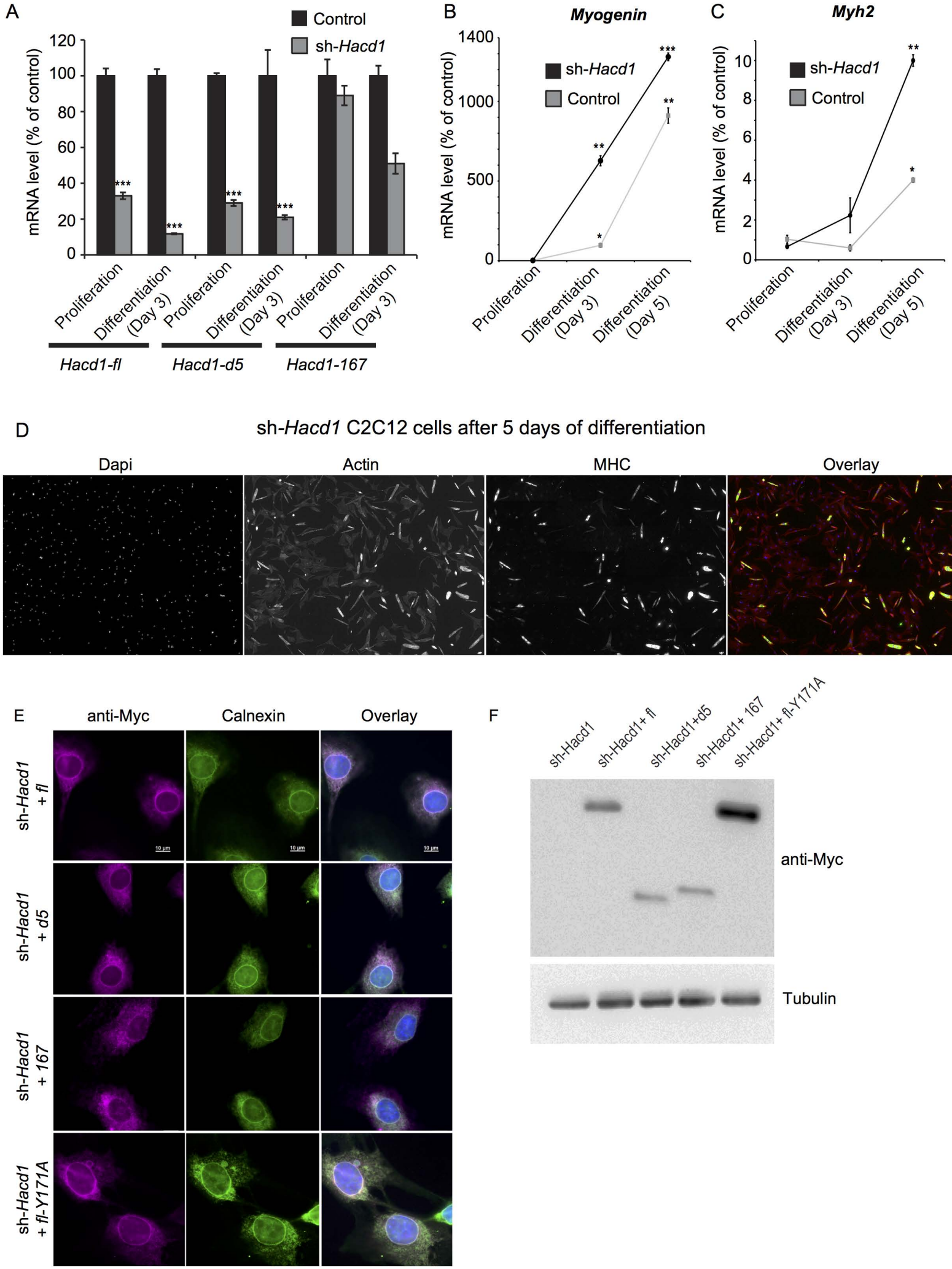

Supplementary Figure 6